DEFORMATION BEHAVIOR OF SANDS UNDER CYCLIC LOADING - A MICRO-STRUCTURAL APPROACH

Final Report on Research
under Contract No. AFOSR-86-0151
sponsored by
United States Air Force
Office of Sceintific Research
Bolling AFB, D.C. 20332-6448

by

Ching.S.Chang
Department of Civil Engineering
University of Massachusetts
Amherst, MA 01003

September 1988

(2)

DEFORMATION BEHAVIOR OF SANDS UNDER CYCLIC LOADING - A MICRO-STRUCTURAL APPROACH

Final Report on Research
sponsored by
United States Air Force
Office of Sceintific Research
Bolling AFB, D.C. 20332-6448

by

Ching.S.Chang

UNCLASSIFIED
SECURITY CLASSIFICATION OF THIS PAGE

REPORT DOCUMENTATION PAGE

Form Approved OMB No. 0704-0188

1a. REPORT SECURITY CLASSIFICATION UNCLASSIFIED	1b. RESTRICTIVE MARKINGS
2a. SECURITY CLASSIFICATION AUTHORITY	3. DISTRIBUTION/AVAILABILITY OF REPORT Approved for Public Release; Distribution Unlimited
2b. DECLASSIFICATION/DOWNGRADING SCHEDULE	
4. PERFORMING ORGANIZATION REPORT NUMBER(S)	5. MONITORING ORGANIZATION REPORT NUMBER(S) AFOSR-TR- 88-0982
6a. NAME OF PERFORMING ORGANIZATION Dept. of Civil Engineering University of Massachusetts (6b. OFFICE SYMBOL (If applicable))	7a. NAME OF MONITORING ORGANIZATION AFOSR/NA
6c. ADDRESS (City, State, and ZIP Code) Amherst, MA 01003	7b. ADDRESS (City, State, and ZIP Code) Bldg. 410 Bolling AFB, DC 20332-6448
8a. NAME OF FUNDING/SPONSORING ORGANIZATION AFOSR (8b. OFFICE SYMBOL (If applicable) NA)	9 PROCUREMENT INSTRUMENT IDENTIFICATION NUMBER AFOSR-86-0151
8c. ADDRESS (City, State, and ZIP Code) Bldg. 410 Bolling AFB, DC 20332-6448	10. SOURCE OF FUNDING NUMBERS PROGRAM ELEMENT NO. 6.1102F; PROJECT NO. 2302; TASK NO C1; WORK UNIT ACCESSION NO.

11. TITLE (Include Security Classification) (U) Deformation Behavior of Sand Under Cyclic Loading - A Microstructural Approach

12. PERSONAL AUTHOR(S)
Ching S. Chang

13a. TYPE OF REPORT	13b. TIME COVERED	14. DATE OF REPORT (Year, Month, Day)	15. PAGE COUNT
Final	FROM 86/4/1 TO 88/8/31	88/9/1	74

16. SUPPLEMENTARY NOTATION

17. COSATI CODES		
FIELD	GROUP	SUB-GROUP

18. SUBJECT TERMS (Continue on reverse if necessary and identify by block number)
Granular Mechanics, Constitutive Law, Packing Structure, Soil Fabric, Random Packings, Soil Moduli, Structural Anisotropy (DFS)

19. ABSTRACT (Continue on reverse if necessary and identify by block number)

The overall objective of this research is to develop a constitutive model for granular materials accounting for its micro-structure. The project focussed on the theoretical development of stress-strain relationship from a micro-mechanics approach, the law governing the force-displacement behavior at a contact under a general cyclic loading condition, and the mathematical characterization of the packing structure in the form of fabric tensor of a granular assembly. Experimental tests were conducted on rod assemblies in a directional shear box to verify the developed theory. Analytical expressions were obtained for the stiffness constants of anisotropic granular assemblies.

20. DISTRIBUTION/AVAILABILITY OF ABSTRACT ☒ UNCLASSIFIED/UNLIMITED ☐ SAME AS RPT ☐ DTIC USERS	21. ABSTRACT SECURITY CLASSIFICATION UNCLASSIFIED
22a. NAME OF RESPONSIBLE INDIVIDUAL Major Steven C. Boyce	22b TELEPHONE (Include Area Code) (202) 767-6963 22c. OFFICE SYMBOL AFOSR/NA

DD Form 1473, JUN 86 Previous editions are obsolete. SECURITY CLASSIFICATION OF THIS PAGE

UNCLASSIFIED

ABSTRACT

The overall objective of this research is to develop a constitutive model for granular materials accounting for its micro-structure. The project focussed on the theoretical development of stress-strain relationship from a micro-mechanics approach, the law governing the force-displacement behavior at a contact under a general cyclic loading condition, and the mathematical characterization of the packing structure in the form of fabric tensor of a granular assembly. Experimental tests were conducted on rod assemblies in a directional shear box to verify the developed theory. Analytical expressions were obtained for the stiffness constants of anisotropic granular assemblies.

TABLE OF CONTENTS

LIST OF FIGURES

Chapter 1

SUMMARY OF THE PROJECT

1.1 RESEARCH OBJECTIVES

The general objective of this research is to study the mechanics of granular material from a micro-structural point of view. The specific objectives of this research are as follows:

1. development of a mathematical model to obtain the stress-strain relationship for a granular material explicitly considering the micro-structure characteristics of the packing,

2. study of the force-displacement law at a contact between two non-conforming bodies and its implementation in the stress-strain relationship,

3. development of the mathematical characterization of the micro-structure of a granular assembly and investigation of its effect on the stiffness characteristics of the packings,

4. experimental study on rod assemblies in a directional shear box to investigate the effects of packing structure and loading conditions on the mechanical behavior of granular assemblies, and

5. verification of the theoretical model by comparing the theoretical results with those from tests on rod assemblies in directional shear box and other available tests in the literature.

1.2 ACCOMPLISHMENTS

1.2.1 Theory

A general mathematical model is developed to evaluate the stress-strain behavior of granular packings based on micro-structural considerations. Two

approaches are followed, namely, (a) mobilized plane approach and (b) particulate approach.

(a) The mobilized plane model assumes that a large number of mobilized planes are developed in a soil element when subject to loading. The overall mechanical behavior of a packing can be obtained based on the movement of the mobilized planes. Work on this approach is given in publications 1, 2, 4 and 7 shown in section 1.3.3.

(b) The particulate model explicitly incorporates the geometrical characteristics of the packing, such as, the void ratio, the coordination number, and the contact normal distribution. The work accomplished in this approach is as follows:

(b.1) The formulation of the stress-strain relationship for regular packings of equal size particles is given in publications 5 and 12 in section 1.3.3.

(b.2) The formulation of the stress-strain relationship for regular packings of multi size particles is given in publication 8 in section 1.3.3.

(b.3) The formulation of the stress-strain relationship for random packings of multi size particles is given in publications 3 and 10 in section 1.3.3.

The theoretical development for the particulate model is discussed in Chapter 2 of this report.

1.2.2 Contact Law

The contact force-displacement law for two non-conforming bodies in contact is incorporated in the stress-strain formulation for the particulate approach. The work accomplished is as follows:

(a) Closed-form solutions of the constitutive matrix for linear contact law are given in publications 6, 9 and 10 in section 1.3.3.

(b) Solutions for non-linear Hertzian-Mindlin contact law are given in publications 6, 9, 10 and 11 in section 1.3.3.

The contact law is discussed in Chapter 3 and the solutions are shown in Chapter 4 and 6 of this report.

1.2.3 Fabric and its Effect on the Mechanical Properties

Mathematical characterization of the micro-structure of a granular assembly is developed. This is incorporated in the stress-strain formulation for the particulate approach to study the effect of packing structure on the stiffness properties. The work accomplished is as follows:

(a) The formulation for representing contact normal distribution and its relationship with the fabric tensor is given in publications 9 and 10 in section 1.3.3.

(b) The stiffness properties of packings with anisotropic micro-structure are given in publications 9, 10 and 11 in section 1.3.3.

The discussion on fabric and its effect on stiffness properties of a packing is given in Chapter 4.

1.2.4 Experiments on Rod Assemblies

Experiments are conducted on assemblies of cylindrical rods to investigate the deformation behavior. The work accomplished is as follows:

(a) Results on directional shear box are given in publications 5, 8 and 13 in section 1.3.3.

(b) Results on model footing tests are given in publication 14 in section 1.3.3.

The experimental results on the directional shear cell is presented in Chapter 5 of this report.

1.2.5 Verification of the Theoretical Model

The theoretical model is verified by comparing the theoretical results with those from the tests in directional shear box and other available test results in the literature. The work accomplished is as follows:

(a) Comparison with results from tests in directional shear box are given in publications 5 and 8 in section 1.3.3.

(b) Comparisons with results on assemblies of glass balls in resonant column device and sands under low amplitude waves are given in publication 11 in section 1.3.3.

The comparisons are discussed in Chapter 6 of this report.

1.3 SUMMARY OF THE PROJECT

1.3.1 Grant Information:

Grant Number : AFOSR-86-0151

Amount: $ 150,489

Period: Apr. 1, 1986 - Aug. 31, 1988

Title: Deformation Behavior for Sands Under Cyclic Loading - A Micro-structural Approach

1.3.2 Professional Personnel Associated with the Project

Principal Investigator: Ching S. Chang

Research Assistants:

Anil Misra (Master's degree completed, Ph.D. in progress)

Gopal C. Biswas (Ph.D. in progress)

Naila M. Hashash (Master's degree completed)

Jia H. Xue (Master's degree completed)

Sivanuja Somasega (Master's degree in progress)

1.3.3 Publications under this grant

Published

1. Chang, C. S., "Behavior of Plastic Flow for Sand," the Second International Conference on Constitutive Law for Engineering Materials: Theory and Application, Tucson, Arizona, Jan., 1987.

2. Chang, C.S., "Micromechanical Approach to Constitutive Modelling for Granular Sand Based on Slip Mechanism," Constitutive Equations for Granular Non-cohesive Soils, A. A. Balkema Publishers, Rotterdam, Netherlands, Edited by Adel S. Saada and G.F. Bianchini, 1988.

3. Chang, C.S., "Micromechanical Modelling of Constitutive Equation for Granular Material," Micromechanics of Granular Materials, Elsevier Science Publishers, Edited by J.T. Jenkins and M. Satake, 1988.(in print)

4. Chang, C. S., Weeraratne, S.P. and Misra, A., "Slip Mechanism Based Constitutive Modelling for Granular Soils," Journal of Engineering Mechanics Division, ASCE. (in print)

5. Chang, C. S. and Misra, A., "Theoretical and Experimental Study of Regular Packings of Granules," Journal of Engineering Mechanics Division, ASCE.(in print)

Submitted

6. Chang, C.S. and Misra, A., "Constitutive Relations for Packings of Spheres," Acta Mechanica, (submitted)

7. Chang, C. S., Weeraratne, S.P. and Misra, A., "Deformation Analysis of Sand in Cubical and Hollow Cylinder Devices," International Journal of Numerical and Analytical Methods in Geomechanics, (submitted)

8. Chang, C. S., Misra, A. and Xue, J.H., "Model Tessellations Applied to Study the Mechanics of Packings Made of Multi-sized Particles," International Journal of Solids and Structures. (submitted)

9. Chang, C. S. and Misra, A., "Influence of Packing Structure on the Mechanics of Granular Matter," Journal of Engineering Mechanics Division, ASCE.(submitted)

10. Chang, C. S. and Misra, A., "Fabric and Stiffness Properties of Anisotropic Granular Packings." Journal of Applied Mechanics, ASME.(submitted)

11. Chang, C. S., Somasegarasundaram, S. and Misra, A., "Implications of Micro-structure on Elastic Moduli of Particulated Mass," International Journal of Numerical and Analytical Methods in Geomechanics, (submitted)

Thesis Completed Under this Grant

12. Misra, A., "Stress-strain Relationship for Simple Models of Sand," Master's Project Report Submitted to the University of Massachusetts in partial fulfillment of the requirements of the degree of Master of Science, 1987.

13. Xue, J.H., "Experimental Study on Mechanical Behavior of Idealized Granular Media," Master's Project Report Submitted to the University of Massachusetts in partial fulfillment of the requirements of the degree of Master of Science, 1988.

14. Hashash, N.M., "Mechanical Response of Two-dimensional Rigid Assemblies," Master's Project Report Submitted to the University of Massachusetts in partial fulfillment of the requirements of the degree of Master of Science, 1988.

1.3.4 Presentations at Conferences

1. The Second International Conference on Constitutive Law for Engineering Materials: Theory and Application, Tucson, Arizona, Jan., 1987.
   - "Behavior of Plastic Flow for Sand,"

2. Engineering Mechanics Division, Specialty Conference, ASCE, Buffalo, New York, May 1987.
   - "A Micro-structural Approach to Constitutive Modelling for Granular Soils,"

3. International Workshop on Constitutive Equations for Granular Non-cohesive Soils, Cleveland, Ohio, July 22-24, 1987.
   - "Micromechanical Approach to Constitutive Modelling for Granular Sand Based on Slip Mechanism,"

4. U.S. Japan Seminar on the Micromechanics of Granular Materials, Sendai, Japan, Oct. 26 - 30, 1987.
   - "Micromechanical Modelling of Constitutive Equation for Granular Material,"

5. Engineering Mechanics Division, Specialty Conference, ASCE, Blacksburg, Virginia, May 1988.
   - "Deformation Analysis for Granular Material,"

6. Engineering Mechanics Division, Specialty Conference, ASCE, Blacksburg, Virginia, May 1988.
   - "Cyclic Stress-strain Modelling for Granular Soils with Micro-structural Consideration,"

Chapter 2

THEORETICAL DEVELOPMENT

The stress-strain modelling of discrete systems, such as granular packings, can only be acheived by considering the continuum field quantities as averages of their discrete analogues (Chang 1987, Chang and Misra 1988b). The stress, a continuum field variable, is related to the discrete contact forces in a granular media. Similarly, the strain in a granular media is related to the contact displacements.

2.1 STRESSES AND CONTACT FORCES

Assembly of spherical particles can be divided into polyhedral sub-volumes defined as 'Voronoi cells' such that the space occupied by the assembly is completely filled (see Fig. 2.1). This polyhedral cell is chosen to contain a particle and the void space closest to that particle (Finney 1970). The average stress tensor $\bar{\sigma}^n_{ij}$ within the nth (see Fig. 2.1) 'Voronoi cell' is given by

$$\bar{\sigma}^n_{ij} = \frac{1}{\Delta V^n} \int \sigma_{ij} \, dv \qquad (2.1)$$

where ΔV^n is the volume of the nth 'Voronoi cell'. From Eq. 2.1 and using the theorem of stress means (Truesdell and Toupin 1960), the average stress tensor for the 'Voronoi cell' is expressed in terms of surface tractions on the 'Voronoi cell' as follows

$$\bar{\sigma}^n_{ij} = \frac{1}{\Delta V^n} \int t_i \, r_j \, ds \qquad (2.2)$$

where t_i is the traction vector on the surface of the nth sub-volume at the location given by the position vector r_j with the origin chosen at the centre of the sphere contained in the nth sub-volume. In a packing of

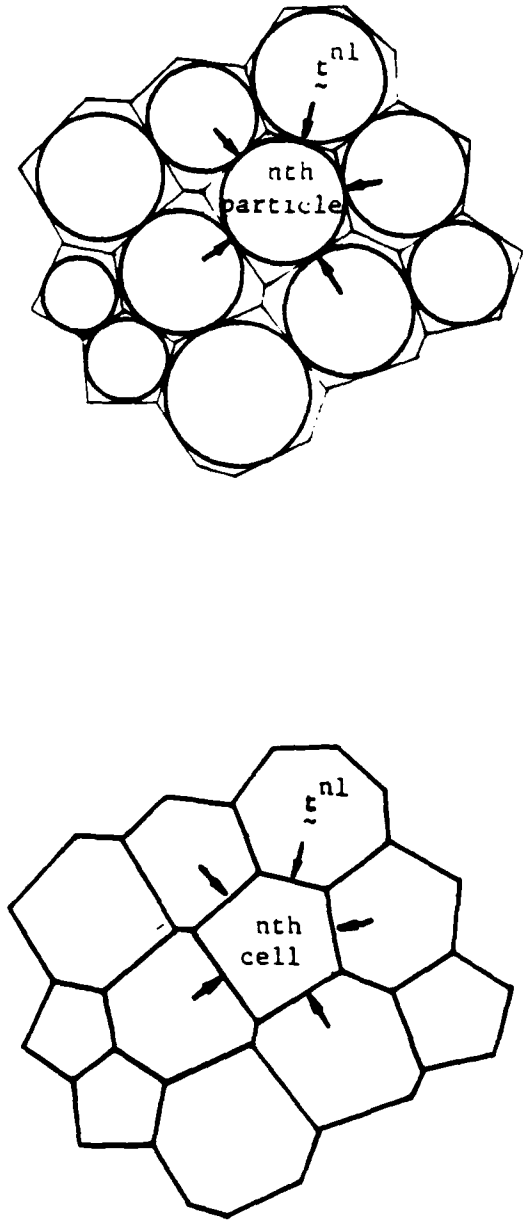

Fig. 2.1 Assembly of spherical particles divided into 'Voronoi' cells.

spheres, instead of continuous surface tractions there are discrete contact points on the surface of the nth sub-volume where the forces act (see Fig. 2.1). Therefore, for this system, Eq. 2.2 reads as

$$\bar{\sigma}^n_{ij} = \frac{1}{\Delta V^n} \sum_m t_i^{nm} r_j^{nm} \tag{2.3}$$

where t_i^{nm} is the contact force at the mth contact of the nth particle and r_j^{nm} represents the position vector of that contact.

For continuum modelling of packings of spheres, it is necessary to define the stress for a representative volume which best represents the packing. This representative volume comprises ot many 'Voronoi cells' of the packing. Clearly, the stress field in an assembly of spheres, due to its discrete nature, is heterogeneous, that is, the average stress $\bar{\sigma}^n_{ij}$ of the 'Voronoi cell' varies from one cell to another. Therefore, in this case, a 'mean' stress tensor for a chosen representative volume may be defined. The 'mean' stress tensor, for this representative volume, is defined as an average of the stress tensors of its sub-volumes ('Voronoi cell') as follows,

$$\langle \sigma_{ij} \rangle = \frac{1}{V} \sum_n \bar{\sigma}^n_{ij} \Delta V^n \tag{2.4}$$

where $\bar{\sigma}^n_{ij}$ is the average stress tensor for the sub-volumes ΔV^n and the volume V is given by

$$V = \sum_n \Delta V^n \tag{2.5}$$

Further, substituting Eq. 2.3 into Eq. 2.4, the 'mean' stress tensor of the medium can be written as

$$\langle \sigma_{(ij)} \rangle = \frac{1}{V} \sum_n \sum_m t^{nm}_{(i} r^{nm}_{j)} \tag{2.6}$$

where () represents the symmetric part. The skew symmetric part, given by,

$$\langle \sigma_{[ij]} \rangle = \frac{1}{V} \sum_n \sum_m t^{nm}_{[i} r^{nm}_{j]} \tag{2.7}$$

represents the 'mean' torque of the representative volume contributed by the torque for each sub-volume caused by the contact force t_i^{nm} acting at r_j^{nm}. In absence of any applied torque or couple stresses, the skew symmetric part is expected to be zero in order to satisfy Cauchy's law of balance of angular momentum (Truesdell and Toupin 1960).

It is noted that representation of stress tensor in granular media, similar to Eq. 2.6, have also been developed by Chrisstoffersen et. al. 1981, Rothenburg and Selvadurai 1981, and Kishino 1978 using different arguments.

2.2 KINEMATICS OF GRANULAR MEDIA

2.2.1 Relative displacement between two contacting spheres

Under an increment of loading, the spheres comprising the granular assembly displace from their original position leading to the deformation of the assembly. Each particle in the assembly, in general, has two modes of movement, namely, translational movement denoted by vector **u** and rotational movement denoted by ω. These movements are accompanied by the interactions at the contact between two particles. Assuming the particles to be rigid, the relative displacement at a contact between two particles, n and p (see Fig. 2.2), can be expressed by

$$\delta = (u^n - u^p) + (\omega^n \times r^n) + (\omega^p \times r^p) \qquad (2.8)$$

where the first term on the right hand side of Eq. 2.8 is contributed by the translation, while the other terms are from particle spin. Further, the relative displacement δ can be expressed as

$$\delta = \delta^{nm} + \delta^{pm} \qquad (2.9)$$

where δ^{nm} and δ^{pm} are the relative displacements associated with particles n and p respectively, and superscript m represents the contact between n and

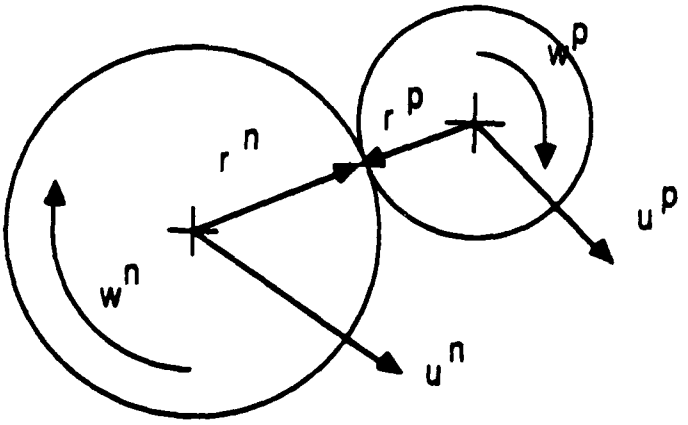

Fig. 2.2 Displacement of two particles in contact.

p. The relative displacement δ has, in general, two components, namely, the normal relative displacement and the shear relative displacement.

2.2.2 Strain tensor

Similar to the stress field, the strain field in a packing of spheres is, in general, inhomogeneous and discontinuous. Analogous to the 'mean' stress tensor, a 'mean' strain tensor can be established for the chosen representative volume. The 'mean' strain tensor for the representative volume is defined from energy equivalence, which states, in general terms, that the work done expressed in terms of the 'mean' stress and 'mean' strain tensor is same as the work done expressed in terms of the contact forces and the relative displacements at the contacts.

The work done, for the representative volume V, expressed in terms of the 'mean' stress and the 'mean' strain is given by

$$dW = V \langle \sigma_{(ij)} \rangle \langle \dot{\varepsilon}_{ij} \rangle \qquad (2.10)$$

where $\langle \dot{\varepsilon}_{ij} \rangle$ is the increment of the symmetric 'mean' strain tensor. By definition, the increment of symmetric 'mean' strain tensor is related to the increment of displacement gradient $\langle D_{ij} \rangle$ and the increment of the rotational tensor $\langle \Omega_{ij} \rangle$ as follows,

$$\langle \dot{\varepsilon}_{ij} \rangle = \langle D_{ij} \rangle - \langle \Omega_{ij} \rangle \qquad (2.11)$$

Needless to say that, as the stress tensor is symmetric, the rotational tensor $\langle \Omega_{ij} \rangle$ (i.e., the anti-symmetric part of the displacement gradient) does not contribute to the work done, dW.

The work done expressed in terms of the contact forces and the incremental relative displacements at the contacts for the same representative volume, is given by

$$dW = \sum_{n} \sum_{m} t_i^{nm} \delta_i^{nm} \tag{2.12}$$

Equating Eq. 2.10 and 2.12 and substituting the expression for $\langle \sigma_{(ij)} \rangle$ from Eq. 2.6, one obtains the relationship between the relative displacement and the 'mean' strain tensor

$$\delta_i^{nm} = r_j^{nm} \langle \varepsilon_{ij} \rangle \tag{2.13}$$

Using Eq. 2.11, Eq. 2.13 can be further written in terms of the displacement gradient tensor and the rotation tensor as follows

$$\delta_i^{nm} = r_j^{nm} \langle D_{ij} \rangle - r_j^{nm} \langle \Omega_{ij} \rangle \tag{2.14}$$

2.2.3 Particle spin and rotation tensor

In Eq. 2.14, δ_i^{nm} represents the relative displacement at the mth contact of the nth ball with respect to its contacting neighbor p considering that the pth ball does not move. Further, by definition, the relative displacement of the nth and the pth balls, compatible with the displacement gradient field D_{ij}, is

$$u^n - u^p = r_j^{nm} \langle D_{ij} \rangle - r_j^{pm} \langle D_{ij} \rangle \tag{2.15}$$

Thus comparing Eqs. 2.8, 2.14 and 2.15, the following relationship is obtained between the particle spin and the rotation tensor,

$$r^n \times \omega^n + r^p \times \omega^p = \left[r_j^{nm} + r_j^{pm} \right] \langle \Omega_{ij} \rangle \tag{2.16}$$

Eq. 2.16 represents an underlying assumption that the mean particle spin is same as the 'mean' rigid body rotation Ω_{ij} of the representative volume.

2.3 RELATION BETWEEN INCREMENTAL STRESS AND STRAIN

2.3.1 Local constitutive law

A local constitutive law relating the incremental contact force and the relative displacement at the contact is defined. For convenience, the local constitutive law is defined in a local cartesian coordinate system

formed by the base vectors **n**, **s** and **t**. Where **n** is the unit normal vector at the mth contact and **s** and **t** are chosen arbitrarily in general (Fig. 2.3). Let T_{ik}^{nm} denote the transformation between the local coordinate system and the global coordinate system such that

$$d_j^{nm} = T_{ik}^{nm}\, \delta_k^{nm}, \quad \text{and} \quad f_i^{nm} = T_{ik}^{nm}\, t_k^{nm} \tag{2.17}$$

where f_i^{nm} and t_k^{nm} are the force increments at the mth contact of the nth particle in the local and global coordinate system respectively, d_j^{nm} and δ_k^{nm} are the relative displacements increment at the mth contact of the nth particle in the local and global coordinate system respectively. The transformation tensor T_{jk}, from the global to the local coordinate system, is given by

$$T_{jk} = e_k^{(j)} \tag{2.18}$$

where $e^{(j)} = \{\mathbf{n}, \mathbf{s}, \mathbf{t}\}$ is a set of basis vector forming the local coordinate system, such that $e^{(1)}=\mathbf{n}$, $e^{(2)}=\mathbf{s}$, and $e^{(3)}=\mathbf{t}$. Vector **n** is defined as

$$\mathbf{n} = (\cos\gamma,\ \sin\gamma\cos\beta,\ \sin\gamma\sin\beta) \tag{2.19}$$

s is given by

$$\mathbf{s} = (-\sin\gamma,\ \cos\gamma\cos\beta,\ \cos\gamma\sin\beta) \tag{2.20}$$

and **t** by

$$\mathbf{t} = (0,\ -\sin\beta,\ \cos\beta) \tag{2.21}$$

where γ and β are defined in Fig. 2.3.

If the local constitutive law is defined in the local coordinate system as follows,

$$f_i^{nm} = K_{ij}^{nm}\, d_j^{nm} \tag{2.22}$$

where K_{ij}^{nm} is the stiffness tensor. Then, in the global coordinate system, the local constitutive law reads as follows,

$$t_l^{nm} = T_{li}^{nm}\, K_{ij}^{nm}\, T_{jk}^{nm}\, \delta_k^{nm} \tag{2.23}$$

2.3.2 Constitutive law for the packing

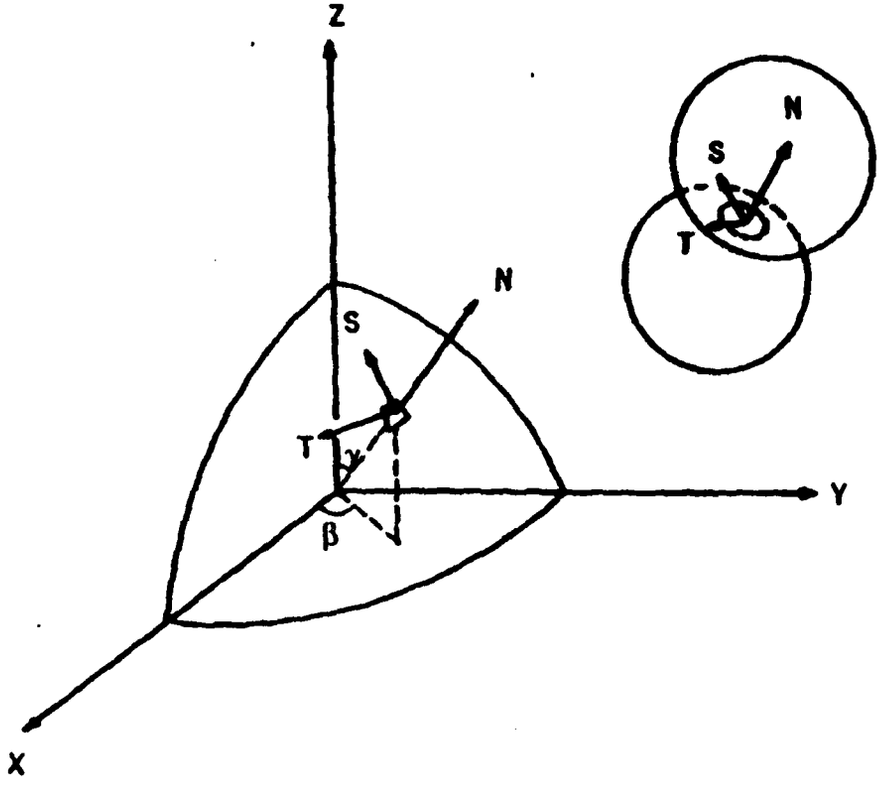

Fig. 2.3 Local coordinate system.

Using the local constitutive law defined above, the overall constitutive relationship of a packing of spheres can be derived. Substituting for δ_k^{nm} from Eq. 2.13 and multiplying by the position vector r_q^{nm} on both sides, Eq. 2.23 becomes

$$r_q^{nm}\, t_l^{nm} = r_q^{nm}\, T_{li}^{nm}\, K_{ij}^{nm}\, T_{jk}^{nm}\, r_p^{nm}\, \langle \dot{\varepsilon}_{kp} \rangle \tag{2.24}$$

Summing up on both sides of Eq. 2.24 and dividing by volume V, the relationship between incremental stress and the incremental strain is obtained as follows

$$\langle \dot{\sigma}_{lq} \rangle = C_{lqkp}\, \langle \dot{\varepsilon}_{kp} \rangle \tag{2.25}$$

where

$$C_{lqkp} = \frac{1}{V} \sum_n \sum_m r_q^{nm}\, T_{li}^{nm}\, K_{ij}^{nm}\, T_{jk}^{nm}\, r_p^{nm} \tag{2.26}$$

and the incremental stress is defined as

$$\langle \dot{\sigma}_{lq} \rangle = \frac{1}{V} \sum_n \sum_m t_l^{nm}\, r_q^{nm} \tag{2.27}$$

It can be shown that the incremental stress and the incremental strain in Eq. 2.26 are frame indifferent quantities, thus satisfying the principle of material objectivity. For example, let Q be any orthogonal transformation tensor from coordinate system $\mathbf{X} \rightarrow \mathbf{X}^*$, such that

$$t_a^{nm^*} = Q_{ai}\, t_i^{nm}; \quad r_b^{nm^*} = r_j^{nm}\, Q_{jb} \tag{2.28}$$

where $t_a^{nm^*}$ and $r_b^{nm^*}$ are in the transformed coordinate system. Then the transformed incremental stress is given by

$$\langle \dot{\sigma} \rangle^* = \mathbf{Q}^t \langle \dot{\sigma} \rangle \mathbf{Q} = \frac{1}{V} \sum_n \sum_m t_a^{nm^*}\, r_b^{nm^*} \tag{2.29}$$

implying that the incremental stress defined in Eq. 2.27 is a frame indifferent quantity under any orthogonal transformation. Similarly the incremental strain can also be shown to be a frame independent quantity.

2.4 INCREMENT OF 'MEAN' STRESS TENSOR AND INCREMENTAL STRESS

The increment of the 'mean' stress tensor is defined as

$$\langle \Delta\sigma_{ij} \rangle = \langle \sigma_{ij} \rangle - \langle \sigma^{o}_{ij} \rangle \tag{2.30}$$

where $\langle \sigma_{ij} \rangle$ and $\langle \sigma^{o}_{ij} \rangle$ are the 'mean' stress tensors in the deformed and the original configurations respectively. Clearly, the incremental stress $\langle \dot{\sigma}_{ij} \rangle$, defined in Eq. 2.27, is not same as the increment of the 'mean' stress tensor. In order to express the constitutive equation in terms of the increment of 'mean' stress tensor, the relation between the incremental stress and the increment of the 'mean' stress tensors needs to be established.

From Eq. 2.6, the 'mean' stress tensors in the deformed and the original configurations respectively are given by

$$\langle \sigma_{ij} \rangle = \frac{1}{V} \sum_{n} \sum_{m} t_i \, r_j, \text{ and } \langle \sigma^{o}_{ij} \rangle = \frac{1}{V^{o}} \sum_{n} \sum_{m} t^{o}_i \, r^{o}_j \tag{2.31}$$

The superscript nm has been dropped in Eq. 2.31 for clarity. The contact force t_i and the position vector r_j in the deformed configuration can be expressed in terms of the contact force t^{o}_i and the position vector r^{o}_j in the original configuration as follows

$$t_i = t^{o}_i + \dot{t}_i \tag{2.32}$$

$$r_j = r^{o}_j + \dot{r}_j \tag{2.33}$$

where the dot refers to the incremental change. The incremental change in the position vector $\dot{r}_j$, by definition, is given by

$$\dot{r}_j = \langle D_{ij} \rangle \, r_j \tag{2.34}$$

where $\langle D_{ij} \rangle$ is the Eulerian displacement gradient. Further, the Tr(D) is defined as

$$\mathrm{Tr}(D) = \langle D_{nn} \rangle = 1 - \frac{V^{o}}{V} \tag{2.35}$$

Substituting Eqs. 2.31, 2.32, and 2.33 into Eq. 2.30, using Eqs. 2.34 and 2.35 and neglecting all the quadratic terms, the relation between the increment of the 'mean' stress tensor $\langle \Delta\sigma_{ij} \rangle$ and the incremental stress tensor $\langle \dot{\sigma}_{ij} \rangle$ is obtained as follows

$$\langle \Delta\sigma_{ij} \rangle = \langle \dot{\sigma}_{ij} \rangle + \langle \sigma_{im} \rangle \langle D_{mj} \rangle - \langle \sigma_{ij} \rangle \langle D_{nn} \rangle \qquad (2.36)$$

Eq. 2.36 represents the familiar relationship between the increment of Cauchy stress $\langle \Delta\sigma_{ij} \rangle$ and the increment of first Piola-Kirchoff stress $\langle \dot{\sigma}_{ij} \rangle$ (Truesdell and Noll 1965). If the symmetry of the incremental stress tensor $\langle \dot{\sigma}_{ij} \rangle$ is rendered explicit, Eq. 2.36 becomes

$$\langle \dot{\sigma}_{ij} \rangle = \langle \Delta\sigma_{ij} \rangle - \frac{1}{2} \left[\langle \sigma_{im} \rangle \langle D_{mj} \rangle + \langle \sigma_{jm} \rangle \langle D_{mi} \rangle \right] + \sigma_{ij} \langle D_{nn} \rangle \qquad (2.37)$$

Thus the constitutive equation can be written in terms of the increment of the Cauchy stress tensor as follows

$$\langle \Delta\sigma_{ij} \rangle = C_{ijkl} \langle \varepsilon_{kl} \rangle + \frac{1}{2} \left[\langle \sigma_{im} \rangle \langle D_{mj} \rangle + \langle \sigma_{jm} \rangle \langle D_{mi} \rangle \right] - \sigma_{ij} \langle D_{nn} \rangle \qquad (2.38)$$

For the case of small deformations the increment of the Cauchy stress can be assumed to be same as increment of the first Piola-Kirchoff stress, that is the second and the third terms on the right side of Eq. 2.37 are negligible compared to the first term. In that case, Eq. 2.38 reads

$$\langle \Delta\sigma_{ij} \rangle = C_{ijkl} \langle \varepsilon_{kl} \rangle \qquad (2.39)$$

where C_{ijkl} is same as defined in Eq. 2.26.

2.5 CONSTITUTIVE EQUATION FOR A CONTINUOUS SYSTEM

The constitutive equation discussed thus far is defined for the case of a discrete distribution of the contact position vectors. However, for a random packing, as the number of contacts becomes very large, the contact position vector distribution can be reasonably treated as continuous. A distribution function $\xi(\Omega)$ of the contact position vectors can be defined such that

$$\int_{\Omega} \xi(\Omega)\, d\Omega = 1 \tag{2.40}$$

Thus the summation in Eq. 2.26 can be replaced by integration and the constitutive tensor becomes

$$C_{lqpk} = \frac{N}{V} \int_{\Omega} r_q(\Omega)\, T_{li}(\Omega)\, K_{ij}(\Omega)\, T_{jk}(\Omega)\, r_p(\Omega)\, \xi(\Omega)\, d\Omega \tag{2.41}$$

where N is the total number of contacts in volume V, $d\Omega = \sin\gamma\, d\gamma\, d\beta$ is the differential solid angle associated with a unit sphere with $0 \leq \gamma \leq \pi$ and $0 \leq \beta \leq 2\pi$ and $\xi(\Omega)$ represents the distribution of the contact position vectors in space.

Chapter 3

CONTACT LAW UNDER CYCLIC LOADING

THe force-displacement behavior at a contact significantly effects the stress-strain behavior of a granular packing. The force-displacement law of two non-conforming bodies in contact can be obtained from the Hertz-Mindlin theory of frictional contacts. The normal and the tangential stiffnesses based on this theory are presented. The assumptions of this theory and their consequences on the contact law are discussed.

3.1 NORMAL CONTACT OF TWO NON-CONFORMING SOLIDS

3.1.1 Hertz theory

For two spheres of radii R_i and elastic properties E_i, G_i and ν_i (i=1,2) the classical theory of Hertz relates the normal force N to the relative approach α of the centres of the two contiguous spheres and the radius a of the circular contact area by the following equations (Johnson 1985):

$$\alpha^3 = \frac{9N^2}{16R\,E^2} \tag{3.1}$$

$$a^3 = \frac{3NR}{4E} \tag{3.2}$$

where

$$\frac{1}{R} = \frac{1}{R_1} + \frac{1}{R_2} \tag{3.3}$$

$$\frac{1}{E} = \frac{(1-\nu_1^2)}{E_1} + \frac{(1-\nu_2^2)}{E_2} \tag{3.4}$$

$$\alpha = \frac{a^2}{R} \tag{3.5}$$

As can be seen from Eq. 3.1,

$$N = \frac{4E\,(R\,\alpha^3)^{1/2}}{3} \tag{3.6}$$

The incremental stiffness is defined as

$$k_n = \frac{\Delta N}{\Delta \alpha} = 2E'a \tag{3.7}$$

from Eq. 3.6 using Eq. 3.5.

For two cylinders in contact the normal stiffness at contacts is based on the Hertz-Mindlin theory of frictional contacts with modifications for conditions of local yielding at contacts (Chang and Misra 1988a). The normal contact stiffnesses is given by

$$\frac{1}{K_n} = \frac{1 - \nu}{\pi \tilde{G}} \left[2 \ln (2R/a) - 1 \right] \tag{3.8}$$

where $a = (2\,(1 - \nu)\,N\,R\,/\,\pi\,G)^{1/2}$, G is an equivalent shear modulus less than the elastic shear modulus, ν is the Poisson's ratio, R is the equivalent radius of the cylinders.

3.1.2 Non-Hertzian theory

The assumptions and restrictions made in the Hertz theory of elastic contact are parabolic profiles, frictionless surfaces and elastic half space theory. However the real situation is much more complicated. For example, when two non-conforming elastic bodies having continuous profiles are pressed into contact, the pressure distribution between them is not determined uniquely by the profiles of the bodies within the contact area. Two further conditions have to be satisfied: (1) that the interface should not carry any tension and (2) that the surfaces should not interfere outside the contact area.

Friction at the interface of two non-conforming bodies brought into normal contact plays a part only if the elastic constants of the two materials are different. The mutual contact pressure produces tangential

displacements at the interface as well as normal compression. If the materials of the two solids are dissimilar, the tangential displacements will, in general be different so that slip will take place. Such slip will be opposed by friction and may, to some extent, be prevented. Therefore a central region where the surfaces stick together and regions of slip towards the edge of contact may be expected. If the coefficient of limiting friction was sufficiently high slip may be prevented entirely.

When the limits of elastic behavior have been exceeded and plastic flow has begun, the plastic zone is fully contained by the surrounding material which is still elastic. For bodies having smooth profiles, e.g. cylinders or spheres, the plastic zone lies beneath the surface. In these circumstances the material displaced is accommodated by an elastic expansion of the surrounding solid. The resulting deformations are of approximately the same magnitude as the elastic deformations. However the results of the Hertzian theory needs to be corrected for the yielding.

As the load is increased further, the plastic zone breaks out to the free surface and the displaced material is free to escape by plastic flow to the sides. This is the 'unconstrained' mode of deformation analysed by the theory of rigid-plastic solids. The plastic zone would be expected to break out to the surface and the unconstrained mode become possible when the pressure at the contact reaches the value given by the rigid-plastic theory.

The contact behavior acounting for these Hertzian restrictions and assumptions have been primarily studied by numerical techniques. No simple closed-form solutions of contact deformations or stiffness for non-Hertzian contacts exit in lietrature to the authors knowledge.

3.2 CYCLIC TANGENTIAL LOADING ON CONTACT

For a constant normal force, the effect of a tangential force $T < \mu N$ is to cause 'slip' over part of the contact area. Slip is initiated at the circumference of the circular contact area and, as T increases, an annular area of slip develops spreading radially inwards until, when $T = \mu N$, rigid body sliding occurs. If the tangential force is reduced then the slip in the opposite direction spreads radially inwards from the perimeter of the contact area. Thus, all load reversals cause slip reversals that propagates radially inwards from the perimeter of the contact area, instead of receding the existing slip annulus. Consequently the tangential stiffness is dependent on the loading history.

The tangential stiffness is also dependent on the magnitude of the normal force. Fig. 3.1 shows schematically, the loading, unloading and reloading behavior for values of normal force at the contact. Mindlin and Deresiewicz (1953) have identified several loading sequences involving variations of both normal and tangential forces and developed theoretical solutions for the tangential stiffness.

A general procedure based on Mindlin and Deresiewicz (1953) work has been reported by Thornton and Randall (1987). The procedure is to update the normal force and contact area radius followed by calculating ΔT using the new values of N and a. By reanalysing the loading cases considered by Mindlin and Deresiewicz (1953) it can be shown that for loading, unloading and reloading, the tangential incremental displacement may be expressed as

$$\Delta\delta = \frac{1}{8G\,a}\left[\pm\,\mu\,\Delta N + \frac{\Delta T - \mu\Delta N}{\theta}\right] \qquad (3.9)$$

except when

$$\Delta\delta < \frac{\mu\,\Delta N}{8G\,a} \quad \text{and sign } (\Delta\delta) = \text{sign } (\Delta N) \qquad (3.10)$$

From Eq. 3.9

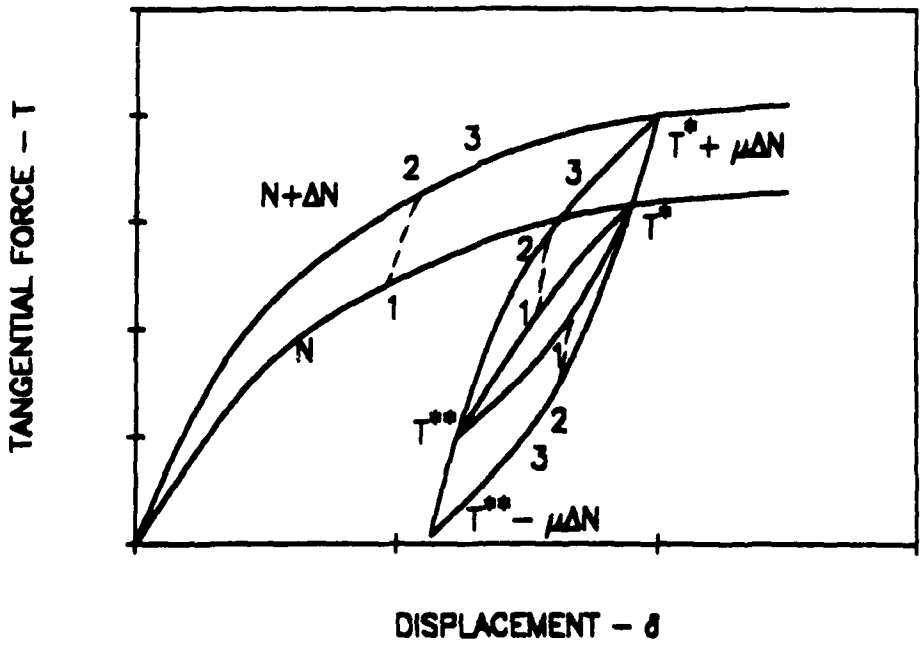

Fig. 3.1 Tangential force versus displacement at a contact.

$$\Delta T = 8G\, a\, \theta\, \Delta\delta \pm \mu \Delta N\, (1-\theta) \tag{3.11}$$

where

$$\frac{1}{G} = \frac{(2 - \nu_1)}{G_1} + \frac{(2 - \nu_2)}{G_2} \tag{3.12}$$

$$\theta^3 = 1 - \frac{(T + \mu \Delta N)}{\mu N} \qquad \text{(loading)} \tag{3.13}$$

$$\theta^3 = 1 - \frac{(T^* - T + 2\mu \Delta N)}{2\, \mu\, N} \qquad \text{(unloading)} \tag{3.14}$$

$$\theta^3 = 1 - \frac{(T - T^{**} + 2\mu \Delta N)}{2\, \mu\, N} \qquad \text{(reloading)} \tag{3.15}$$

and the negative sign in Eq. 3.11 is only evoked during unloading, T^* and T^{**} are defined in Fig 3.1. For a current state given by point 1 in Fig 3.1 (during loading, unloading, or reloading) a tangential incremental displacement corresponding to

$$|\Delta\delta| = \frac{\mu\, |\Delta N|}{8\, G\, a} \qquad \text{with } \Delta N > 0 \tag{3.16}$$

will result in a new state given by point 2 on the curve corresponding to the new value of N. Larger values of $|\Delta\delta|$ will result in a state farther along the curve such as point 3. A problem occurs if the conditions given in Eq. 3.10 is satisfied, since point 2 is not reached and the new state does not lie on the curve corresponding to the new value of N. This case can be solved by setting θ=1 in Eq. 3.11 until $8Ga\Sigma\Delta\delta \geq \mu\Sigma\Delta N$.

For two cylinders in contact the shear stiffness at contacts based on the Hertz-Mindlin theory of frictional contacts with modifications for conditions of local yielding at contacts (Mindlin 1949, Chang and Misra 1988a) is given by

$$\frac{1}{K_s} = \frac{1}{K_n} \Psi \left[1 - T/(\tan \phi_\mu\, N)\right]^{-1/2} \tag{3.17}$$

where ϕ_μ is the friction angle between the two particles, N and T are the normal and shear force at the contact respectively, and Ψ is a constant.

Chapter 4

FABRIC TENSOR AND STIFFNESS PROPERTIES OF RANDOM PACKINGS

Among the significant geometrical features that influence the stress-strain behavior of a granular assembly are the void ratio, the coordination number and the spatial distribution of the vectors joining the centroid of the particle to the contact point on the surface called the contact position vectors. For convenience the distribution function of the contact position vectors can be represented in a tensorial form. The distribution function is related to the 'fabric tensor' of the granular packing. Using this distribution function and assuming a contact force-displacement law the stiffness constants for anisotropic packings of spheres and discs can be obtained (Chang and Misra 1988c, 1988d).

4.1 GEOMETRICAL PROPERTIES OF THE PACKING STRUCTURE

Geometrical properties of granular packings have been of interest in various areas of engineering. Various efforts have been made to identify the geometrical characteristics of importance in the study of granular media in general (Gray 1968, Shahinpoor 1983, Oda et. al. 1982). Studies suggest that among the geometrical properties of granular packings that influence the mechanical behavior are the average coordination number, the void ratio, and the distribution of the contact position vectors in space.

4.1.1 Coordination number and void ratio

For a granular assembly, the coordination number is defined as the number of contact points per particle. The average coordination number of a random assembly is a useful measure of the closeness of the packing or the

void ratio. The void ratio is defined as the ratio of the volume of voids with the volume of solids in a packing. The total number of contacts N in a given volume V of a granular packing can be obtained from the knowledge of the void ratio e, the coordination number $\bar{m}$ and the particle size. For a packing of equal sized particles, the ratio of number of contacts to the volume of the packing, $\frac{N}{V}$, can be expressed as follows

$$\frac{N}{V} = \frac{3\bar{m}}{4\pi\rho^3(1+e)} \text{ (for spheres)}; \quad \frac{N}{V} = \frac{\bar{m}}{\pi\rho^2(1+e)} \text{ (for discs)} \qquad (4.1)$$

where ρ is the particle radius.

Further, the correlation between the coordination number and the void ratio of the packing have been studied experimentally by several investigators (Oda et. al. 1982, Yanagisawa 1983). The relationship between $\bar{m}$ and e have been experimentally found for lead and glass balls by Smith, Foote and Busang (1929), Filep (1936), Field (1963), and Oda (1977). Experimental results are also obtained by Marsal (1973) for rockfill materials and Yanagisawa (1983) for gravels with round and flat shapes. Some of the empirical equations are listed as follows:

1. Yanagisawa (1983) $$\bar{m} = 3.183^{(2.469-e)} \qquad (4.2)$$

2. Smith, et.al. (1929) $$\bar{m} = 26.486 - \frac{10.726}{(1-n)} \qquad (4.3)$$

3. Filep (1936) $$\bar{m} = \frac{3.1}{n} \qquad (4.4)$$

4. Field(1963) $$\bar{m} = \frac{12}{(1+e)} \qquad (4.5)$$

These four empirical equations are plotted in Fig. 4.1 and compared with experimental data. Experimental results from Oda et. al. (1982)

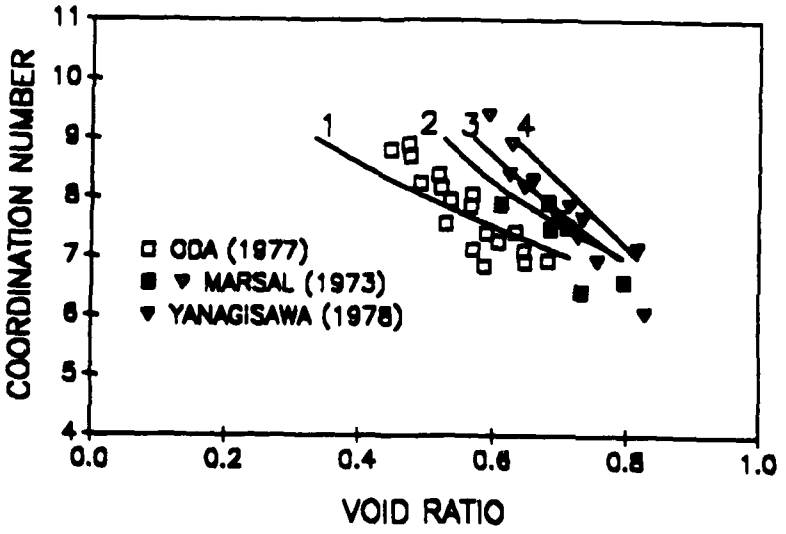

Fig. 4.1 Coordination number $\bar{m}$ vs void ratio e.

suggests that the relation between the coordination number and the void ratio is independent of grain size distribution.

4.1.2 Fabric tensor

Another important measure of the packing structure of granular media is a second order symmetric tensor, termed the 'fabric tensor', that has been introduced by some investigators (Ref. Satake 1982, Oda et. al. 1982, Cowin 1985). More general form of the 'fabric tensor' has been introduced by Kanatani (1984). In general, the 'fabric tensor' represents the average of the tensor product of the observed directional data, such as contact position vectors. The contact position vector is defined as the vector joining the centroid of a particle to a contact point (representing contact with a neighboring particle) on its surface (r^n and r^p in Fig. 2.2). For packings of spherical particles the contact position vector is same as the contact normal vector. If only the unit vector n in the direction of the contact normal vector is considered then, in general, the 'fabric tensor' can be defined as a tensor of rank m given by

$$N_{i_1 i_2 \ldots i_m} = \int_{\Omega} n_{i_1} n_{i_2} \ldots n_{i_m} \, \xi(\gamma,\beta) \, d\Omega = \langle n_{i_1} n_{i_2} \ldots n_{i_m} \rangle \qquad (4.6a)$$

where $\langle\ \rangle$ denotes the ensemble average of the m observed contact normals $n_{i_1}, n_{i_2}, \ldots, n_{i_m}$, $\xi(\gamma,\beta)$ is the density function of the directional distribution of the contact normals, and $d\Omega = \sin\gamma \, d\gamma \, d\beta$ is the differential solid angle associated with a unit sphere with $0 \leq \gamma \leq \pi$ and $0 \leq \beta \leq 2\pi$ (γ and β are defined in Fig. 2.3), such that,

$$N_{i_1 i_2 \ldots i_m} = \int_0^{2\pi} \int_0^{\pi} n_{i_1} n_{i_2} \ldots n_{i_m} \, \xi(\gamma,\beta) \, \sin\gamma \, d\gamma \, d\beta \qquad (4.6b)$$

The 'fabric tensor' defined here is useful in defining the tensorial form of the distribution density function $\xi(\gamma,\beta)$. The relationship between the

'fabric tensor' and the density function $\xi(\gamma,\beta)$ will be discussed in the next section.

4.1.3 Distribution density of contact normals

The empirical distribution of the contact normals in space, for a random granular system, is in general expected to be discrete and random. For continuum modelling of granular packings, it is useful to represent this empirical discrete distribution of contact normals by a smooth density function. Such a directional distribution, in three dimensions, can be expressed as a spherical harmonics expansion given by

$$\xi(\gamma,\beta) = \frac{1}{4\pi}\left[1 + \sum_{k=2}^{\infty}{}'\left\{ a_{k0}\, P_k(\cos\gamma) + \sum_{m=1}^{k} P_k^m(\cos\gamma)\,[a_{km}\cos m\beta + b_{km}\sin m\beta]\right\}\right] \qquad (4.7)$$

where γ and β are defined in Fig. 2.3. Here, Σ' denotes summation with respect to even indices only, $P_k(\cos\gamma)$ is the kth Legendre polynomial, $P_k^m(\cos\gamma)$ is the associated Legendre function and a_{k0}, a_{km}, and b_{km} are parameters. In order to ensure that the density function $\xi(\gamma,\beta)$ is centro-symmetric, i.e. $\xi(\gamma,\beta) = \xi(\pi+\gamma,\beta+\pi)$, only the even harmonics are admissible. It is evident that the first term, i.e. 1, in the expansion, Eq. 4.7, represents a sphere and the subsequent terms can be regarded as a function defined on the surface of the sphere. Further, since the Legendre polynomials and the associated Legendre functions are orthogonal to 1, it follows that the Eq. 4.7 satisfies the identity

$$\int_{\Omega} \xi(\gamma,\beta)\, d\Omega = 1 \qquad (4.8)$$

signifying it is a density function.

Similarly, in two dimensions, the directional distribution can be expanded in form of a Fourier series given by

$$\xi(\theta) = \frac{1}{2\pi}\left[1 + \sum_{k=2}^{\infty}{}' a_k \cos k\theta + b_k \sin k\theta\right] \tag{4.9}$$

Due to the centro-symmetric nature of the distribution, that is $\xi(\theta) = \xi(\theta+\pi)$, only the even terms appear. Clearly, Eq. 4.9 also satisfies the identity $\int_{\theta} \xi(\theta)\, d\theta = 1$.

The expression for the distribution of contact normals, i.e. Eq. 4.7 or 4.9, can be alternatively written as a cartesian tensor equation

$$\xi(\mathbf{n}) = \frac{1}{4\pi}\left[1 + \Phi_{ij}n_i n_j + \Phi_{ijkl}n_i n_j n_k n_l + \cdots\cdots\right] \tag{4.10a}$$

or

$$\xi(\mathbf{n}) = \frac{1}{2\pi}\left[1 + \Phi_{ij}n_i n_j + \Phi_{ijkl}n_i n_j n_k n_l + \cdots\cdots\right] \tag{4.10b}$$

which represents a polynomial in terms of direction cosines of $\mathbf{n}$. In Eq. 4.10, $\Phi_{i_1\cdots i_m}$ is a coefficient tensor of rank m of appropriate choice such that Eq. 4.10 expands to Eq. 4.7 or Eq. 4.9. It is evident that the coefficient tensor $\Phi_{i_1\cdots i_m}$ can be expressed in terms of the coefficients of Eq. 4.7 or 4.9.

Since Eq. 4.7 represents a spherical harmonics expansion, Kanatani (1984) has shown that the coefficient tensor $\Phi_{i_1\cdots i_m}$ is a traceless tensor. He has further shown that the coefficient tensor $\Phi_{i_1\cdots i_m}$ can be determined using the 'fabric tensor' $N_{i_1\cdots i_m}$ and hence is directly related to the packing structure of the assembly. The 'fabric tensor' $N_{i_1 i_2\cdots i_m}$ is related to the coefficient tensor $\Phi_{i_1 i_2\cdots i_m}$. For example, for m=2 the coefficient tensor Φ_{ij} is related to 'fabric tensor' N_{ij} as

$$\Phi_{ij} = \frac{15}{2}\left[N_{ij} - \frac{1}{3}\delta_{ij}\right] \text{ (for spheres)};$$

$$\Phi_{ij} = 4\left[N_{ij} - \frac{1}{2}\delta_{ij}\right] \text{ (for discs)} \tag{4.11}$$

Mathematical details on the spherical harmonics expansion are discussed in (Butkov 1968, Kanatani 1984).

4.2 STIFFNESS CONSTANTS FOR RANDOM PACKINGS

Using the general expression of the constitutive tensor for packings of given by Eq. 2.41, the density function of the form given by Eq. 4.7 or 4.9 and assuming a local constitutive law, the stiffness constants for a random assembly of any packing structure can be obtained.

4.2.1 Constant contact stiffness

Closed form solutions for the stiffness constants are derived by assuming that all contacts in the assembly have the same mechanical property independent of the stress state. A simple diagonal form of the local constitutive matrix K_{ij} relating the relative displacement vector $d_j=(d_n, d_s, d_t)$ and the incremental force vector $f_i=(f_n, f_s, f_t)$ (or $d_j=(d_n, d_s)$ and $f_i=(f_n, f_s)$ in two dimensions) is assumed, such that, $K_{11}= K_n$, $K_{22}=K_{33}=K_s$ and $K_{ij}= 0$ $(i\neq j)$. K_n and K_s are the normal and the shear stiffness respectively at the contact. It is assumed that there is no coupling between the shear and the normal forces at the contact such that the off diagonal terms of the local constitutive matrix are zero ($K_{ij}=0$ for $i\neq j$).

4.2.1.1 Packings of equal spheres

For the simplicity of further derivation, a truncated form of the expansion in Eq. 4.7. consisting of second order terms is used. The Legendre polynomial of degree 2, i.e. $P_2(\cos\gamma)$, is given by (Abramowitz and Stegun 1965)

$$P_2(\cos\gamma) = \frac{1}{2}(3\cos^2\gamma - 1) \qquad (4.12)$$

The associated Legendre function $P_2^2(\cos\gamma)$ can be obtained from the Rodrigues formula (Abramowitz and Stegun 1965)

$$P_k^m(x) = \frac{(1 - x^2)^{m/2}}{2^k\, k!} \frac{d^{k+m}}{dx^{k+m}} (x^2 - 1)^k \tag{4.13}$$

For k=2 and m=2, Eq. 4.13 yields

$$P_2^2(\cos\gamma) = 3 \sin^2\gamma \tag{4.14}$$

Thus the truncated expansion is given as

$$\xi(\gamma,\beta) = \frac{1}{4\pi} \left[1 + \frac{1}{4} a_{20} (3 \cos 2\gamma + 1) + 3 \sin^2\gamma (a_{22}\cos 2\beta + b_{22}\sin 2\beta) \right] \tag{4.15}$$

Alternatively, writing Eq. 4.15 as a cartesian tensor equation

$$\xi(\mathbf{n}) = \frac{1}{4\pi} \left[1 + \Phi_{ij} n_i n_j \right] \tag{4.16}$$

where $\mathbf{n} = (\cos\gamma, \sin\gamma\cos\beta, \sin\gamma\sin\beta)$, and the coefficient tensor Φ_{ij} is given by

$$[\Phi_{ij}] = \begin{bmatrix} a_{20} & 0 & 0 \\ 0 & -\frac{1}{2} a_{20} + 3a_{22} & 3b_{22} \\ 0 & 3b_{22} & -\frac{1}{2} a_{20} - 3a_{22} \end{bmatrix} \tag{4.17}$$

The first term in Eq. 4.16, clearly, represents the isotropic portion of the distribution while the second term represents the anisotropic part. For brevity, the isotropic and the anistropic parts can be combined as follows

$$\xi(\mathbf{n}) = \frac{1}{4\pi} \left[(\delta_{ij} + \Phi_{ij})\, n_i n_j \right] = \frac{1}{4\pi} \left[F_{ij}\, n_i n_j \right] \tag{4.18}$$

where F_{ij} is a generalized 'fabric tensor' that characterizes the distribution function of the normal vectors at the contacts. Substituting Eq. 4.18 into Eq. 2.41, the constitutive tensor becomes

$$C_{lqpk} = \frac{r^2 N}{4\pi V} \int_0^{2\pi} \int_0^{\pi} n_q\, T_{li}\, K_{ij}\, T_{jk}\, n_p\, F_{rs}\, n_r n_s \sin\gamma\, d\gamma\, d\beta \tag{4.19}$$

Taking into account the symmetry of the incremental stress and strain tensors, the stress-strain relationship, equivalent to Eq. 4.19, can be expressed in Voigt's notation as follows,

$$\langle \dot{\sigma}_m \rangle = C_{mn} \langle \dot{\varepsilon}_n \rangle \tag{4.20}$$

where

$\langle \dot{\sigma}_m \rangle = (\dot{\sigma}_{zz}, \dot{\sigma}_{yy}, \dot{\sigma}_{xx}, \dot{\sigma}_{zy}, \dot{\sigma}_{zx}, \dot{\sigma}_{xy})$

and

$\langle \dot{\varepsilon}_n \rangle = (\dot{\varepsilon}_{zz}, \dot{\varepsilon}_{yy}, \dot{\varepsilon}_{xx}, 2\dot{\varepsilon}_{zy}, 2\dot{\varepsilon}_{zx}, 2\dot{\varepsilon}_{xy})$

The stiffness constants C_{mn} for a packing fabric of a 2^{nd} order spherical expansion form (Eq. 4.15) are given as

$$C_{11} = \frac{r^2 N}{15 V} \left[(3K_n + 2K_s) + \frac{2a_{20}}{7} (6K_n + K_s) \right] \tag{4.21}$$

$$C_{22} = \frac{r^2 N}{15 V} \left[(3K_n + 2K_s) - \frac{a_{20}}{7} (6K_n + K_s) + \frac{6a_{22}}{7} (6K_n + K_s) \right] \tag{4.22}$$

$$C_{33} = \frac{r^2 N}{15 V} \left[(3K_n + 2K_s) - \frac{a_{20}}{7} (6K_n + K_s) - \frac{6a_{22}}{7} (6K_n + K_s) \right] \tag{4.23}$$

$$C_{12} = \frac{r^2 N}{15 V} \left[(K_n - K_s) + \frac{a_{20}}{7} (K_n - K_s) + \frac{6a_{22}}{7} (K_n - K_s) \right] \tag{4.24}$$

$$C_{13} = \frac{r^2 N}{15 V} \left[(K_n - K_s) + \frac{a_{20}}{7} (K_n - K_s) - \frac{6a_{22}}{7} (K_n - K_s) \right] \tag{4.25}$$

$$C_{23} = \frac{r^2 N}{15 V} \left[(K_n - K_s) - \frac{2a_{20}}{7} (K_n - K_s) \right] \tag{4.26}$$

$$C_{44} = \frac{r^2 N}{30 V} \left[(2K_n + 3K_s) + \frac{a_{20}}{7} (2K_n + \frac{3}{2} K_s) + \frac{6a_{22}}{7} (2K_n + \frac{3}{2} K_s) \right] \tag{4.27}$$

$$C_{55} = \frac{r^2 N}{30 V} \left[(2K_n + 3K_s) + \frac{a_{20}}{7} (2K_n + \frac{3}{2} K_s) - \frac{6a_{22}}{7} (2K_n + \frac{3}{2} K_s) \right] \tag{4.28}$$

$$C_{66} = \frac{r^2 N}{30 V} \left[(2K_n + 3K_s) - \frac{2a_{20}}{7} (2K_n + \frac{3}{2} K_s) \right] \tag{4.29}$$

$$C_{16} = \frac{r^2 N}{30 V} \left[\frac{12b_{22}}{7} (K_n - K_s) \right] \tag{4.30}$$

$$C_{26} = \frac{r^2 N}{30 V} \left[\frac{12 b_{22}}{7} (3K_n + \frac{1}{2} K_s) \right] \quad (4.31)$$

$$C_{36} = \frac{r^2 N}{30 V} \left[\frac{12 b_{22}}{7} (3K_n + \frac{1}{2} K_s) \right] \quad (4.32)$$

$$C_{45} = \frac{r^2 N}{30 V} \left[\frac{12 b_{22}}{7} (K_n + \frac{3}{4} K_s) \right] \quad (4.33)$$

The other elements of the stiffness matrix C_{mn} are zeros. The ratio of number of contacts to the volume of the packing, $\frac{N}{V}$, is expressed in terms of the coordination number $\bar{m}$ and void ratio e by Eq. 4.1.

4.2.1.2 **Packings of equal disks**

For simplicity, a truncated form of the Fourier expansion in Eq. 4.9 with terms upto fourth order are used. The truncated expansion is given as

$$\xi(\theta) = \frac{1}{2\pi} \left[1 + a_2 \cos 2\theta + b_2 \sin 2\theta + a_4 \cos 4\theta + b_4 \sin 4\theta \right] \quad (4.34)$$

Alternatively, Eq. 4.34 can be written as a cartesian tensor equation

$$\xi(\mathbf{n}) = \frac{1}{4\pi} \left[1 + \Phi_{ij} n_i n_j + \Phi_{ijkl} n_i n_j n_k n_l \right] \quad (4.35)$$

where $\mathbf{n} = (\cos\theta, \sin\theta)$.

Taking into account the symmetry of the incremental stress and strain tensors, the stress-strain relationship, equivalent to Eq. 4.19, can be expressed in Voigt's notation as follows,

$$\langle \dot{\sigma}_m \rangle = C_{mn} \langle \dot{\varepsilon}_n \rangle \quad (4.36)$$

where $\langle \dot{\sigma}_m \rangle = (\dot{\sigma}_{yy}, \dot{\sigma}_{xx}, \dot{\sigma}_{yx})$ and $\langle \dot{\varepsilon}_n \rangle = (\dot{\varepsilon}_{yy}, \dot{\varepsilon}_{xx}, 2\dot{\varepsilon}_{yx})$.

The stiffness constants C_{mn} are given as

$$C_{11} = \frac{\bar{n}}{8\pi (1+e)} \left[(6K_n + 2K_s) + 4a_2 K_n + a_4 (K_n - K_s) \right] \quad (4.37)$$

$$C_{22} = \frac{\bar{n}}{8\pi (1+e)} \left[(6K_n + 2K_s) - 4a_2 K_n + a_4 (K_n - K_s) \right] \quad (4.38)$$

$$C_{12} = \frac{\bar{n}}{8\pi\,(1+e)} \left[2\,(K_n - K_s) - a_4\,(K_n - K_s) \right] \tag{4.39}$$

$$C_{33} = \frac{\bar{n}}{16\pi\,(1+e)} \left[4\,(K_n + K_s) - 2a_4\,(K_n - K_s) \right] \tag{4.40}$$

$$C_{13} = \frac{\bar{n}}{16\pi\,(1+e)} \left[2b_2\,K_n + b_4\,(K_n - K_s) \right] \tag{4.41}$$

$$C_{23} = \frac{\bar{n}}{16\pi\,(1+e)} \left[2b_2\,(K_n + K_s) - b_4\,K_n \right] \tag{4.42}$$

It is noted that for the case of isotropic packing structure, i.e. $a_2=a_4=b_2=b_4=0$, Eqs. 4.37-4.42 yield similar results as Bathurst and Rothenburg (1987).

4.2.2 Hertzian-Mindlin Contact

Under the condition for which the shear force does not exceed the frictional strength at a contact, the local constitutive law can also be defined based on frictional Hertzian-Mindlin contact. The contact stiffnesses, K_n and K_s, obtained from the Hertz-Mindlin theory for frictional contacts (Mindlin and Deresiewicz 1953) are given in Chapter 3.

If, instead of a linear local constitutive law, a non-linear Hertzian-Mindlin contact law is assumed, the expressions of C_{mn} become very complex and the close form solutions can only be obtained for the case of statistically isotropic packing under initial isotropic stress condition.

For a statistically isotropic packing, the contact force vector f, under initial isotropic stress ($\sigma_{ij} = P\delta_{ij}$), is the same for all contacts, given by

$$f_n = \frac{3\,V\,P}{r\,N}; \quad f_s = f_t = 0 \tag{4.43}$$

Thus using Eqs. 4.21-4.33 with $a_{20}=a_{22}=b_{22}=0$, the Poisson's ratio and the Young's modulus for the packing are given as

$$\nu_{iso} = \frac{\nu}{2\ (5-3\nu)} \tag{4.44}$$

$$E_{iso} = \frac{4\ r^2\ (5-4\nu)}{30\quad (5-3\nu)}\left[\ 9P\ \right]^{1/3}\left[\ \frac{G\ N}{(1\ -\ \nu)\ V}\ \right]^{2/3} \tag{4.45}$$

For other packings and initial loading conditions other than isotropic, the expressions become very complex and a numerical approach to the solutions is more tractable.

4.3 TYPES OF MATERIAL SYMMETRY

Due to the different packing structure, a granular assembly may, conceivably, exhibit different types of material symmetries. The forms of the stiffness matrix for various types of material symmetries are shown in Table 4.1 (Nye 1957). Evidently, the various types of material symmetries can be represented by an appropriate choice of the 'fabric tensor' F_{ij}. Along with the forms of stiffness matrix for the different material symmetries the corresponding 'fabric tensor' F_{ij} are presented in Table 1.

The packing structure of a granular packing with orthotropic material symmetry non-coincident with the stress axes can be represented by a second rank symmetric fabric tensor with three non-zero parameters a_{20}, a_{22}, and b_{22}. A granular packing in this case will have 13 independent non-zero stiffness constants given by Eqs. 4.21 to 4.33. It is noted that for this material the normal stresses σ_{zz}, σ_{yy}, σ_{xx} are coupled with the shear strain ε_{xy}.

Granular packings with orthotropic material symmetry can be represented by a diagonal second rank fabric tensor with two non-zero parameters a_{20} and a_{22}. Orthotropic material is characterized by symmetry

TABLE - 1 Forms of stiffness matrices C_{mn} and the fabric tensor F_{ij} for various material symmetries

Stiffness Matrix C_{mn}	Fabric tensor F_{ij}
Orthotropic with non-coincident stress axes $\begin{bmatrix} * & * & * & . & . & * \\ & * & * & . & . & * \\ & & * & . & . & * \\ & \text{symm} & & * & * & . \\ & & & & * & . \\ & & & & & * \end{bmatrix}$	$\begin{bmatrix} 1 + a_{20} & 0 & 0 \\ 0 & 1 - \frac{1}{2} a_{20} + 3a_{22} & 3b_{22} \\ 0 & 3b_{22} & 1 - \frac{1}{2} a_{20} - 3a_{22} \end{bmatrix}$
Orthotropic $\begin{bmatrix} * & * & * & . & . & . \\ & * & * & . & . & . \\ & & * & . & . & . \\ & \text{symm} & & * & . & . \\ & & & & * & . \\ & & & & & * \end{bmatrix}$	$\begin{bmatrix} 1 + a_{20} & 0 & 0 \\ 0 & 1 - \frac{1}{2} a_{20} + 3a_{22} & 0 \\ 0 & 0 & 1 - \frac{1}{2} a_{20} - 3a_{22} \end{bmatrix}$
Tetragonal $\begin{bmatrix} * & *\!\!-\!\!* & * & . & . & . \\ & *\diagdown & * & . & . & . \\ & & *\diagdown & . & . & . \\ & \text{symm} & & *\diagdown & . & . \\ & & & & *\diagdown & . \\ & & & & & * \end{bmatrix}$	$\begin{bmatrix} 1 + a_{20} & 0 & 0 \\ 0 & 1 + a_{20} & 0 \\ 0 & 0 & 1 - 2a_{20} \end{bmatrix}$
Transverse isotropic $\begin{bmatrix} * & *\!\!-\!\!* & * & . & . & . \\ & *\diagdown & * & . & . & . \\ & & *\diagdown & . & . & . \\ & \text{symm} & & *\diagdown & . & . \\ & & & & *\diagdown & . \\ & & & & & o \end{bmatrix}$	$\begin{bmatrix} 1 + a_{20} & 0 & 0 \\ 0 & 1 - \frac{1}{2} a_{20} & 0 \\ 0 & 0 & 1 - \frac{1}{2} a_{20} \end{bmatrix}$
Isotropic $\begin{bmatrix} *\diagdown & *\!\!-\!\!* & * & . & . & . \\ & *\diagdown & * & . & . & . \\ & & *\diagdown & . & . & . \\ & \text{symm} & & o\diagdown & . & . \\ & & & & o\diagdown & . \\ & & & & & o \end{bmatrix}$	$\begin{bmatrix} 1 & 0 & 0 \\ 0 & 1 & 0 \\ 0 & 0 & 1 \end{bmatrix}$

. - zero components, * - non-zero components, o - $\frac{1}{2}(C_{22} - C_{23})$, *——* - equal components

about three mutually orthogonal planes. The stiffness matrix of materials with orthotropic symmetry is represented by 9 independent constants. For orthotropic materials the normal stresses are not coupled with the shear strains and the vice versa.

Granular packings with tetragonal material symmetry have 6 independent stiffness constants. Tetragonal symmetry is characterized by a an axis of symmetry. If the parameters defining the fabric tensor F_{ij} were chosen such that $a_{20} = 2a_{22}$ and $b_{22}=0$, then packings with tetragonal symmetry can be represented.

In addition to possessing an axis of symmetry, certain granular assemblies, have an additional condition on the stiffness constants, that is $C_{66} = \frac{1}{2}(C_{22} - C_{23})$. The number of independent constants characterizing the stiffness matrix for such packings are thus reduced to 5. This type of material symmetry is termed transverse isotropic symmetry. The fabric tensor for the transverse isotropic material can be represented by choosing $a_{22}=b_{22}=0$.

If the fabric tensor is chosen such that $a_{20}=a_{22}=b_{22}=0$, then packings with isotropic material properties can be represented. It is noted that the stiffness constants for packings with different material symmetry can be obtained from Eqs. 4.21 to 4.33 by using appropriate values of a_{20}, a_{22} and b_{22}.

4.4 DISCUSSION

To demonstrate the effect of packing anisotropy on the mechanical properties of random packings, parametric studies are performed for the statistically isotropic, transverse isotropic and orthotropic packings. Fig. 4.2 shows the density functions $\xi(n)$ of the contact normal vectors for

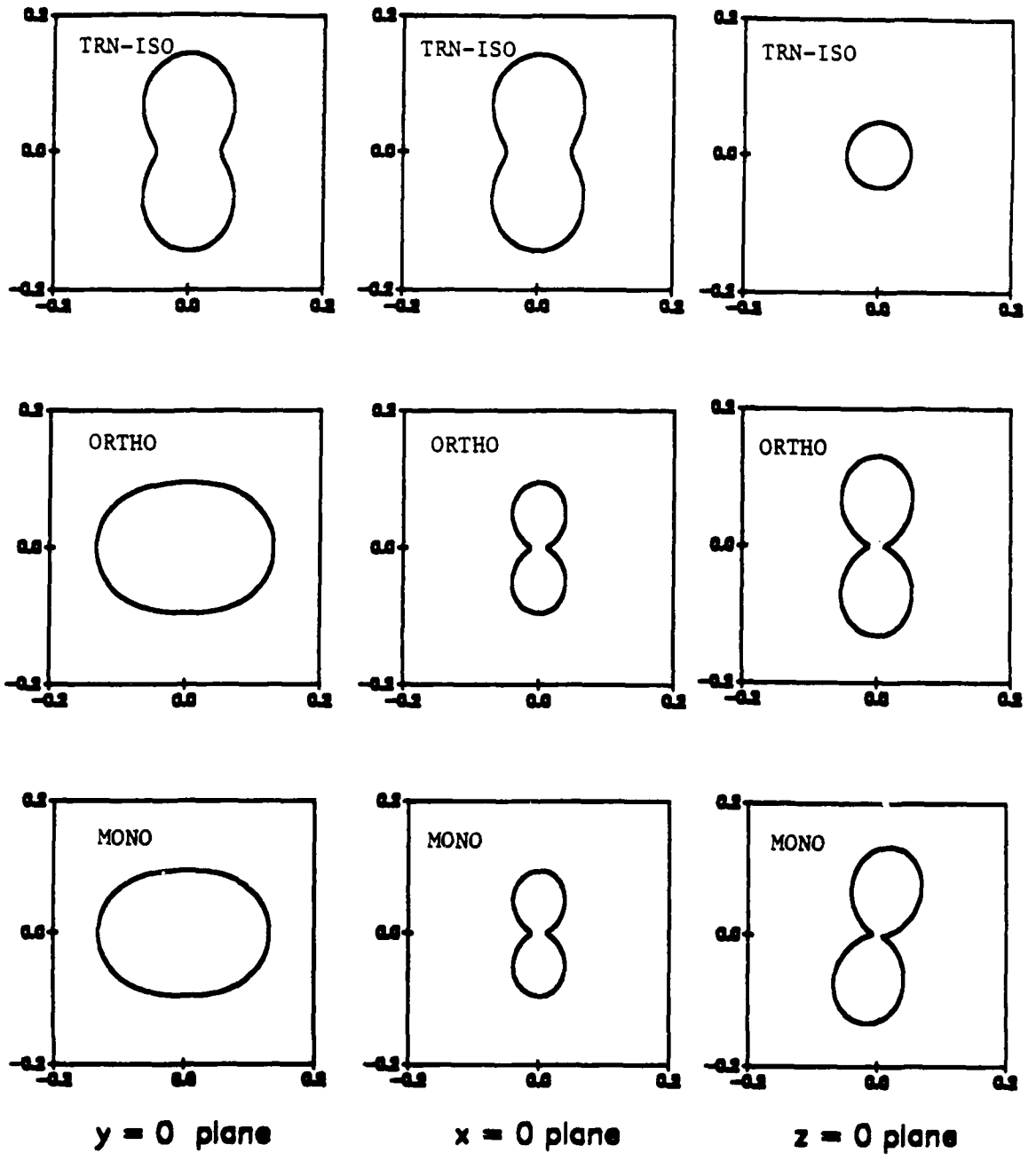

Fig. 4.2 Section of density function $\xi(n)$ for statistically transverse isotropic, orthotropic, and monoclinic packings along $x=0$, $y=0$, and $z=0$ planes.

the monoclinic, the orthotropic and the transverse isotropic packings. Three sections of the density function, along x=0, y=0, and z=0 planes respectively, are plotted in Fig. 4.2. The following values of the parameters are used for this plot: a_{20}= 0.8, a_{22}=b_{22}=0 for transverse isotropic packing, a_{20}= 0.2, a_{22}=0.25, b_{22}=0 for orthotropic packing, and a_{20}= 0.2, a_{22}=0.25, b_{22}=0.1 for monoclinic packing.

The solutions are computed based on Eqs. 4.21 to 4.33 using the following values for the parameters: $\bar{n}$ = 9, e = 0.57, r=0.01 in., and K_n= 3800 psi. Fig. 4.3 shows the Young's modulus and the Poisson's ratio plotted against the ratio K_s/K_n (the shear stiffness K_s to the normal stiffness K_n) for statistically isotropic packing. As expected, the Young's modulus increases and the Poisson's ratio decreases with the ratio K_s/K_n. The maximum value for the Poisson's ratio is 0.25 when the ratio K_s/K_n is zero for perfectly smooth spheres with no tangential interactions.

Figs. 4.4, 4.5 and 4.6 show the variation of the Young's moduli, the Poisson's ratios, and the shear moduli, respectively, with the ratio K_s/K_n for the transverse isotropic and the orthotropic packings. The Young's moduli E_{xx}=E_{yy} and E_{zz}, the two Poisson's ratios ν_{zx}=ν_{zy} and ν_{xy}, and the shear moduli G_{zx}=G_{zy} and G_{xy} for the transverse isotropic are computed for the parameter a_{20}=0.8. It is noted that the shear modulus G_{xy} can be expressed in terms of E_{xx} and ν_{xy}, thus there are only 5 independent constants for the transverse isotropic packing. The three Young's moduli E_{xx}, E_{yy} and E_{zz}, the three Poisson's ratio ν_{zx}, ν_{zy} and ν_{xy}, and the three shear moduli G_{zx}, G_{zy} and G_{xy} for the orthotropic packings are plotted for the value of the parameter a_{20}=0.2 and parameter a_{22}=0.25.

To show the effect of degree of anisotropy on the mechanical properties, the ratios of Young's moduli for transverse isotropic packing to

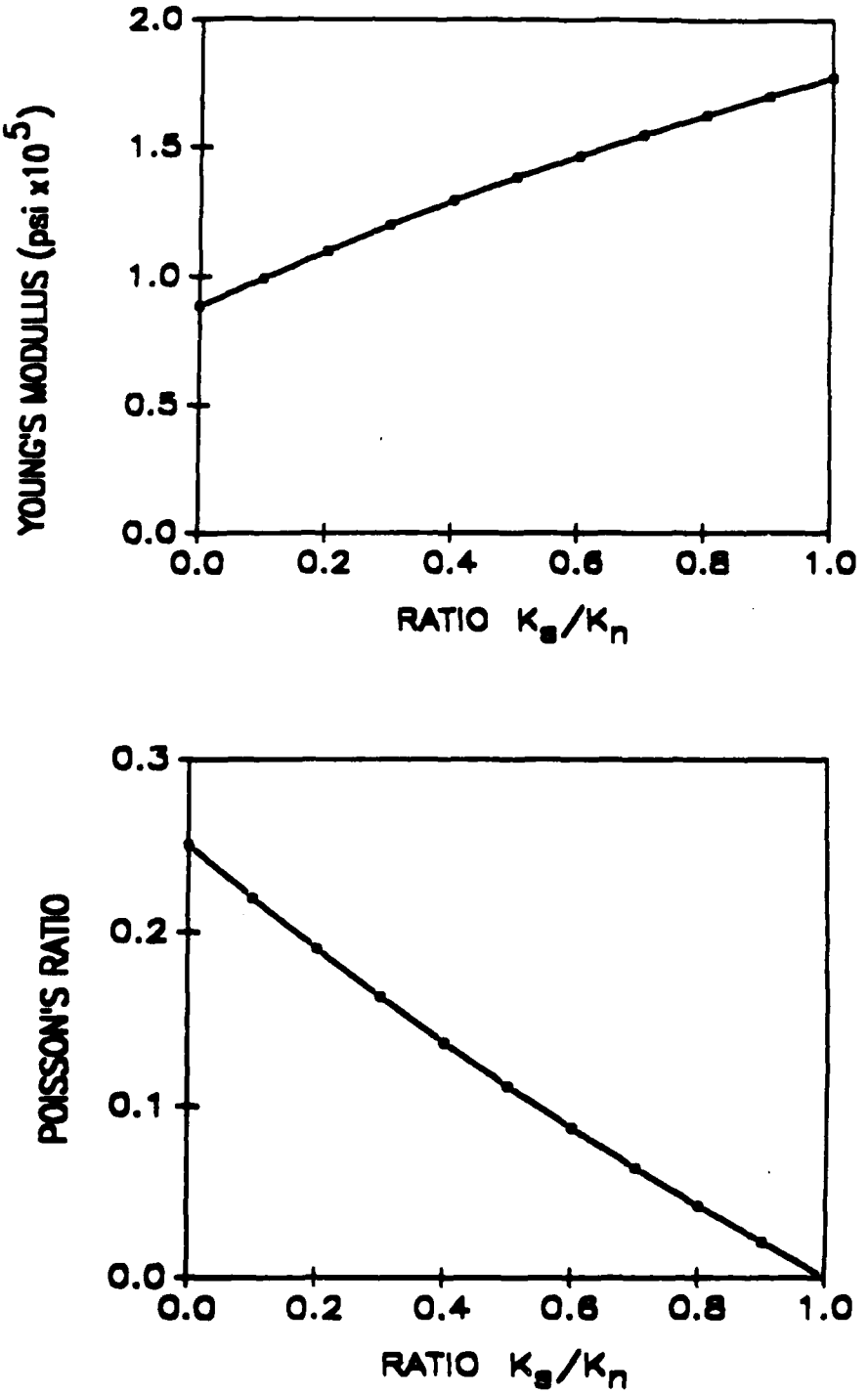

Fig. 4.3 Variation of Young's modulus and Poisson's ratio with the ratio K_s/K_n for statistically isotropic packings.

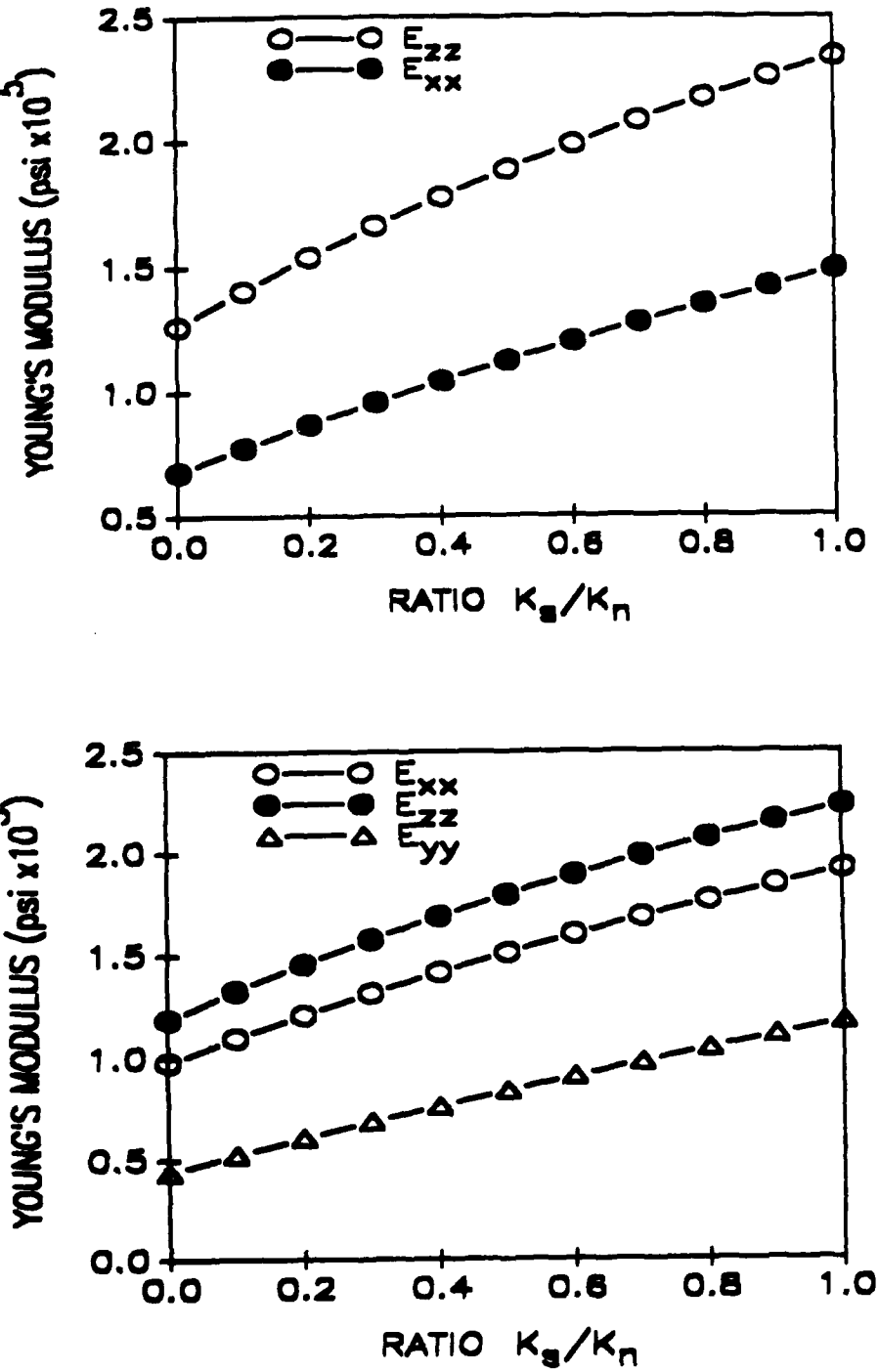

Fig. 4.4 Variation of Young's moduli with the ratio K_s/K_n for statistically transverse isotropic and orthotropic packings respectively.

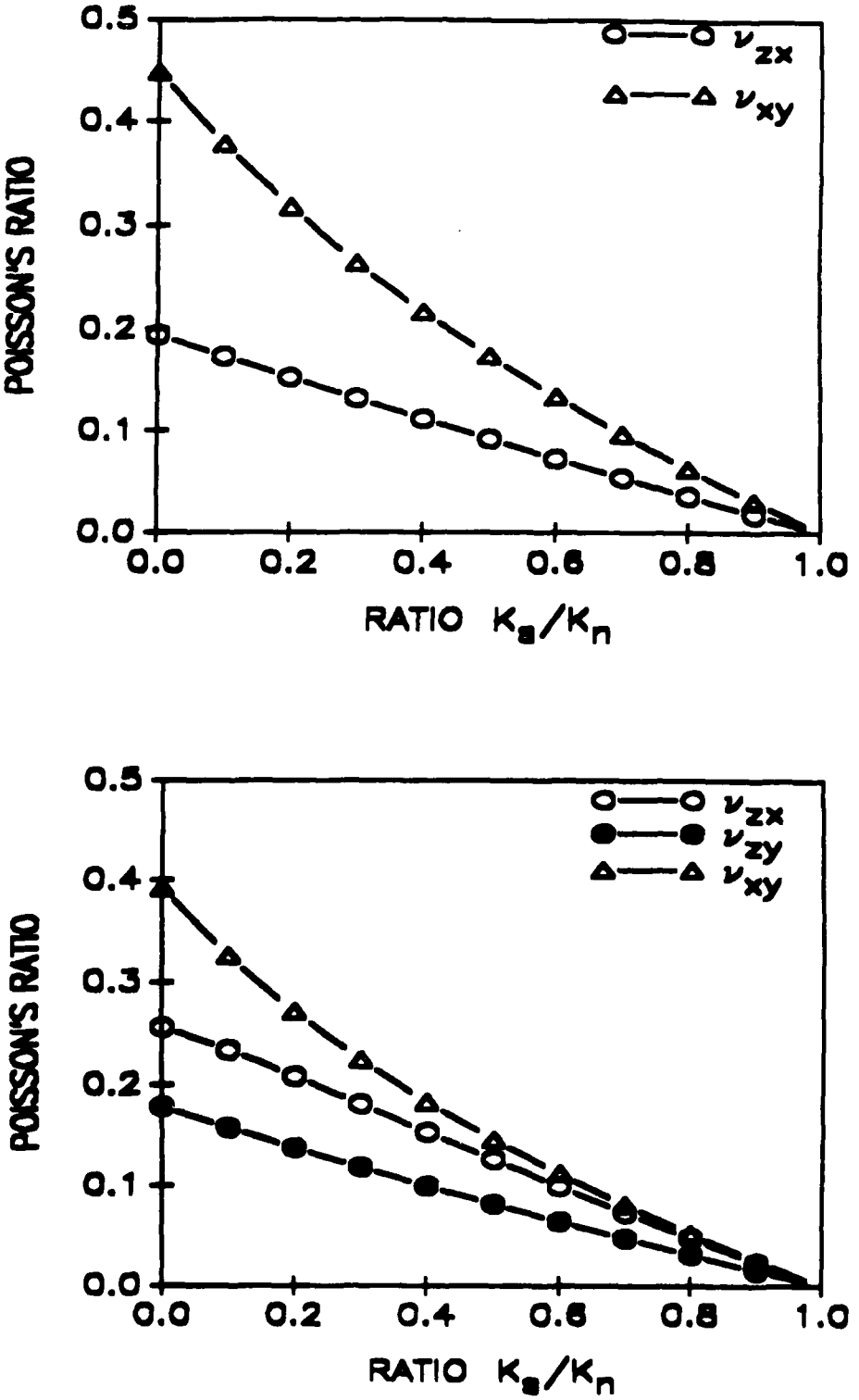

Fig. 4.5 Variation of Poisson's ratio with the ratio K_s/K_n for statistically transverse isotropic and orthotropic packings respectively.

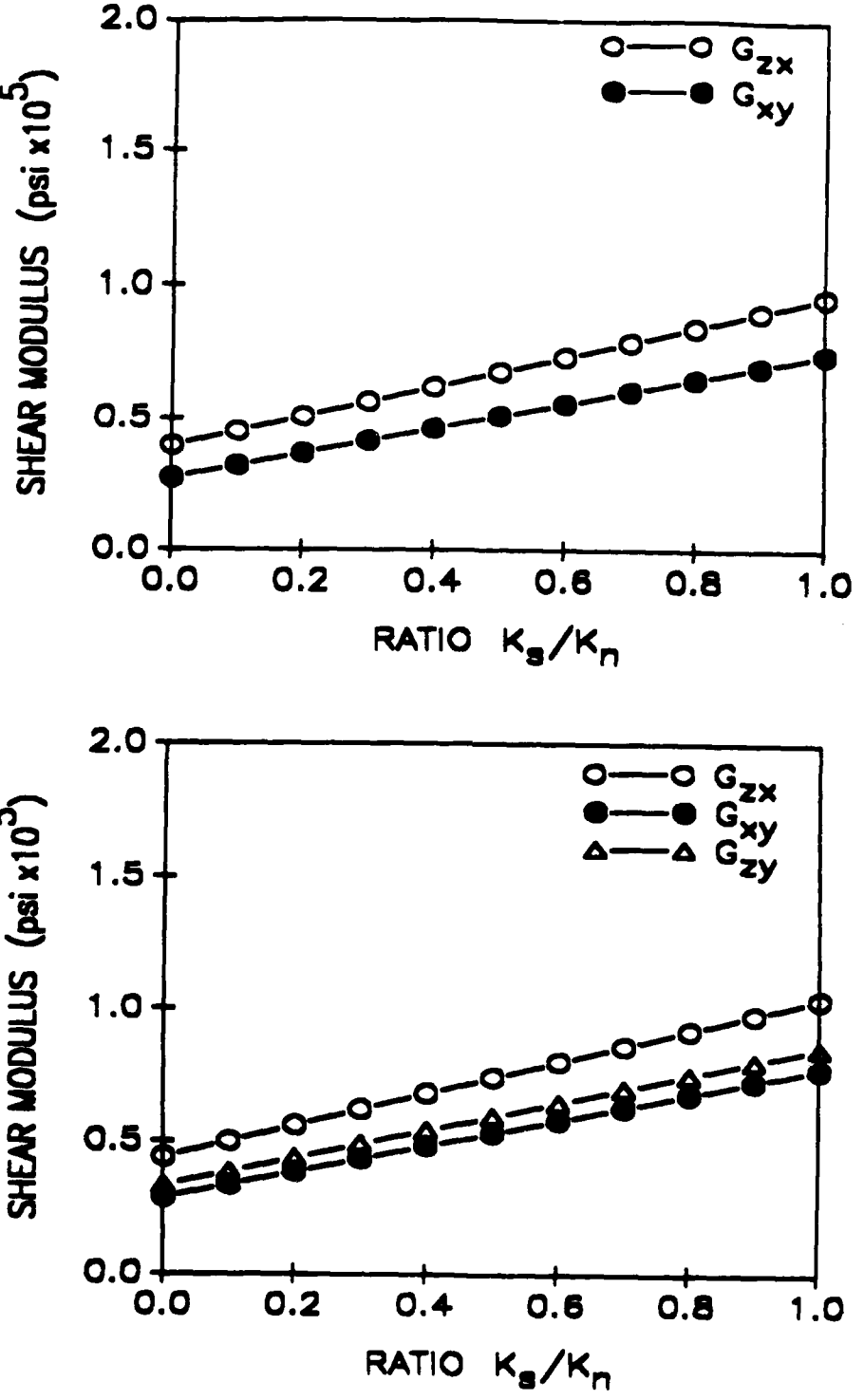

Fig. 4.6 Variation of Shear moduli with the ratio K_s/K_n for statistically transverse isotropic and orthotropic packings respectively.

the Young's modulus for isotropic packing are plotted against the parameter a_{20} in Fig. 4.7. The ratios of the Poisson's ratios for the two packings are also shown in Fig. 4.7. Clearly the more anisotropic packing structure has a more anisotropic mechanical properties.

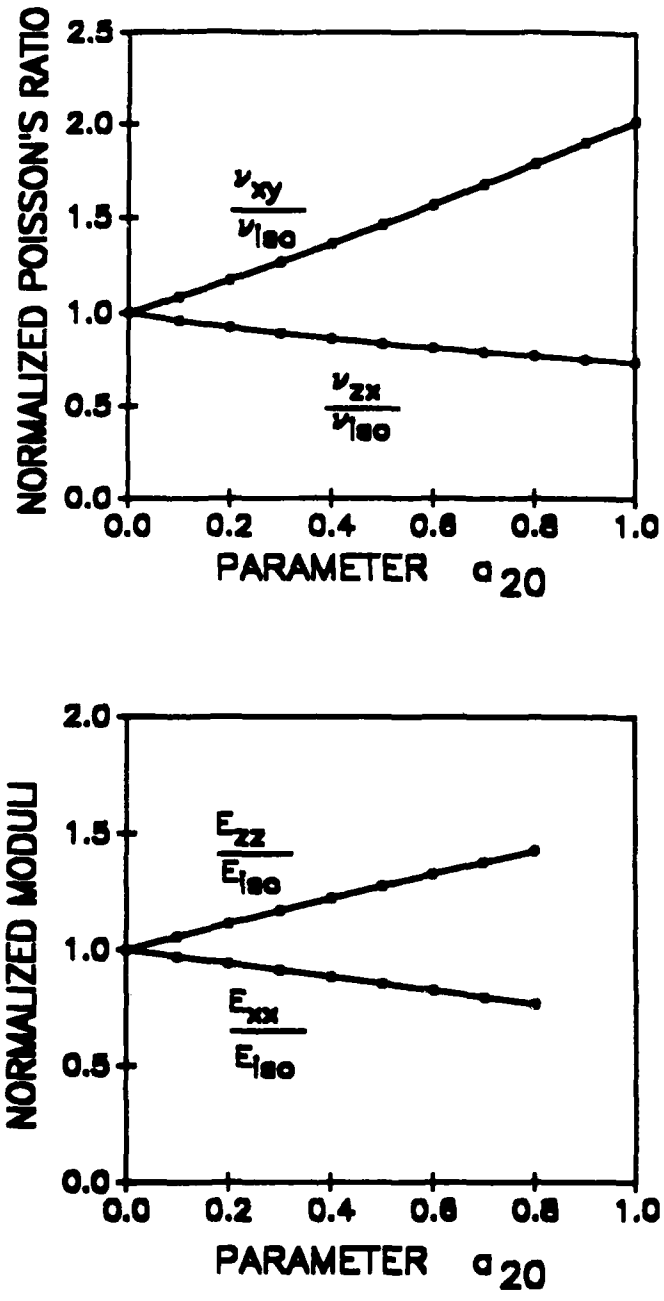

Fig. 4.7 Ratios of Young's moduli and Poisson's ratio for statistically transverse isotropic packings to the Young's moduli and Poisson's ratio for statistically isotropic packings respectively with the parameter a_{20}.

Chapter 5

EXPERIMENTAL STUDY ON ROD ASSEMBLIES

Experimental tests were performed to provide a database for the verification of the developed theory. Experiments were performed to obtain stress-strain response of packings with regular and random structures. Specifically of interest was the directional dependence of the stiffness properties of the packings. Details of the experimental setup are presented in Xue 1988.

5.1 APPARATUS

The apparatus used in this study consists of a loading frame composed of 4 rigid aluminium plates 1/2" thick and 2" high. The maximum size of rods assembly that can be placed in the loading frame is 8" by 8" in dimension. Each rod of assembly is placed vertically, resting on a glass table top (shown in Fig. 5.1). The frame is so designed that it can be compressed independently in X and Y directions. The box can also be made to swing about Y-axis, hence it can serve as a directional shear box.

The loading is applied using a set of push-pull type pneumatic cylinders (or pistons) controlled by regulators with air pressure gages attached. Cylinders can be pulled or pushed to apply compressive forces and shear forces to this box with desired stress conditions, such as: isotropic compression, biaxial compression, and shear loading with a controlled rotation of principal stress axis. Five dial gages that read to 0.0001" are attached (see Fig. 5.1) to monitor deformations.

5.2 SPECIMENS AND MEASUREMENTS

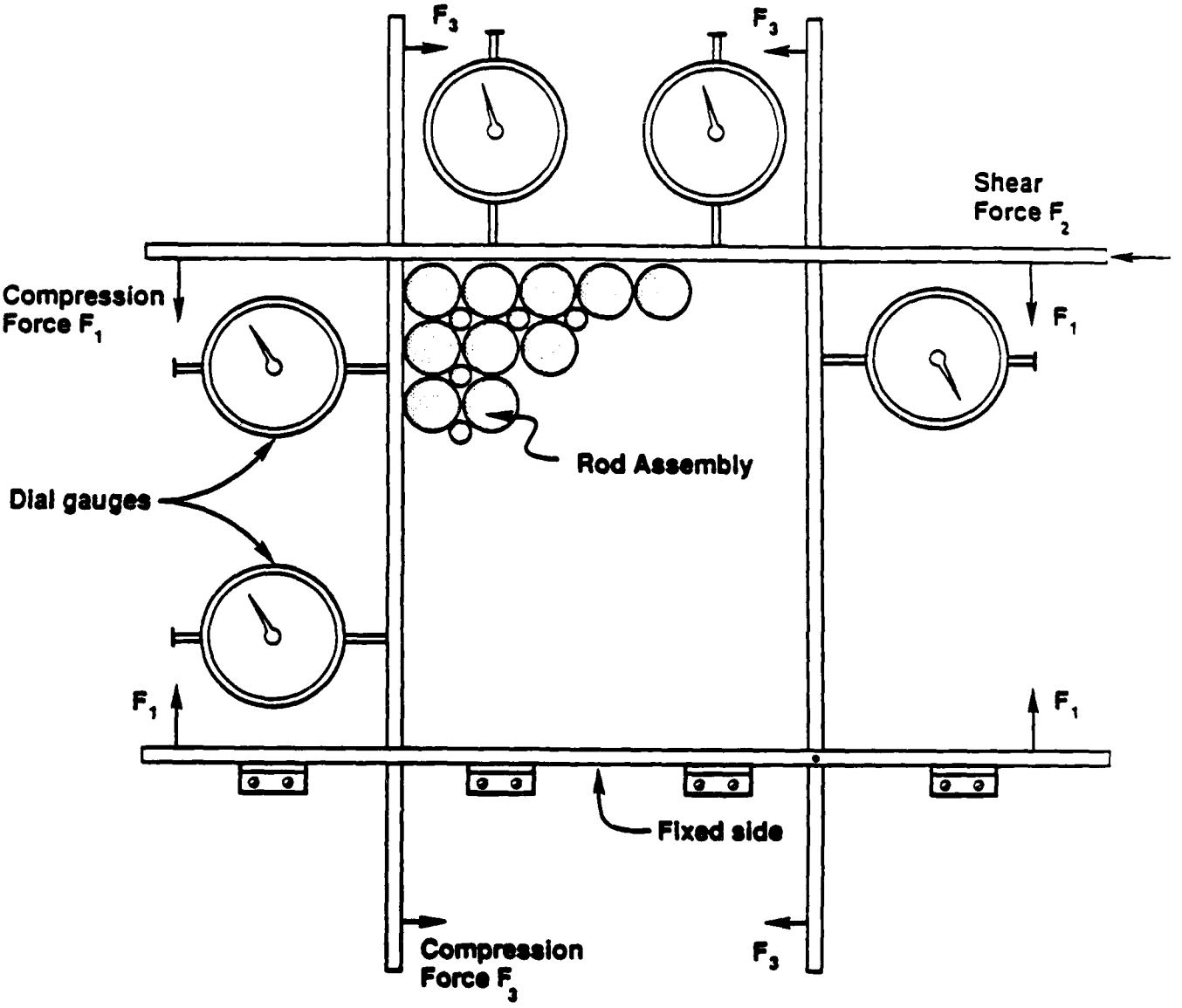

Fig. 5.1 The directional shear box.

Six regular and two random packings have been investigated. Samples of approximately 300 aluminum cylinders, of 2 in. high, are placed randomly or in accordance with a given regular packing arrangement.

Regular packing structres selected in this study consist of four packings of equal sized cylinders and two packings of multi-sized cylinders as shown in Fig. 5.2. For packing A, B, C and D, the diameter of the cylinders used is 0.5 inch. For packing E, the diameters of the cylinders used are 0.5 inch and 0.25 inch, and for packing F, 0.75 inch and 0.5 inch. Two types of random packings are used, namely one sized packing made of 271 rods of 0.5 in. diameter and two sized packing made of 229 rods of 0.5 in. diameter and 190 rods of 0.25 in. diameter.

Strains of the rods assembly is obtained from the deformation of the box measured from the attached 5 dial gages. The thickness of the frame plates is designed to be large enough such that the bending deflection of the loading frame is insignificant.

Stresses applied on the rods sample are calculated from the readings of the pressure gages connected to the pneumatic cylinders. Since the actual forces transmitted to the rods assembly are different from those directly calculated from pressure gages due to friction loses in the system, calibration was made to account for the friction loses in the piston of the pneumatic cylinders and the friction loses between the loading frame and the glass plate. In addition, the stress madnitude applied to the assembly was selected to be much larger than the friction between rods and the smoothened glass plate so that the effect of friction is expected to be insignificant.

Photographs of the assembly packing were taken for the random assembly. The rods are painted black on the top and their centers are

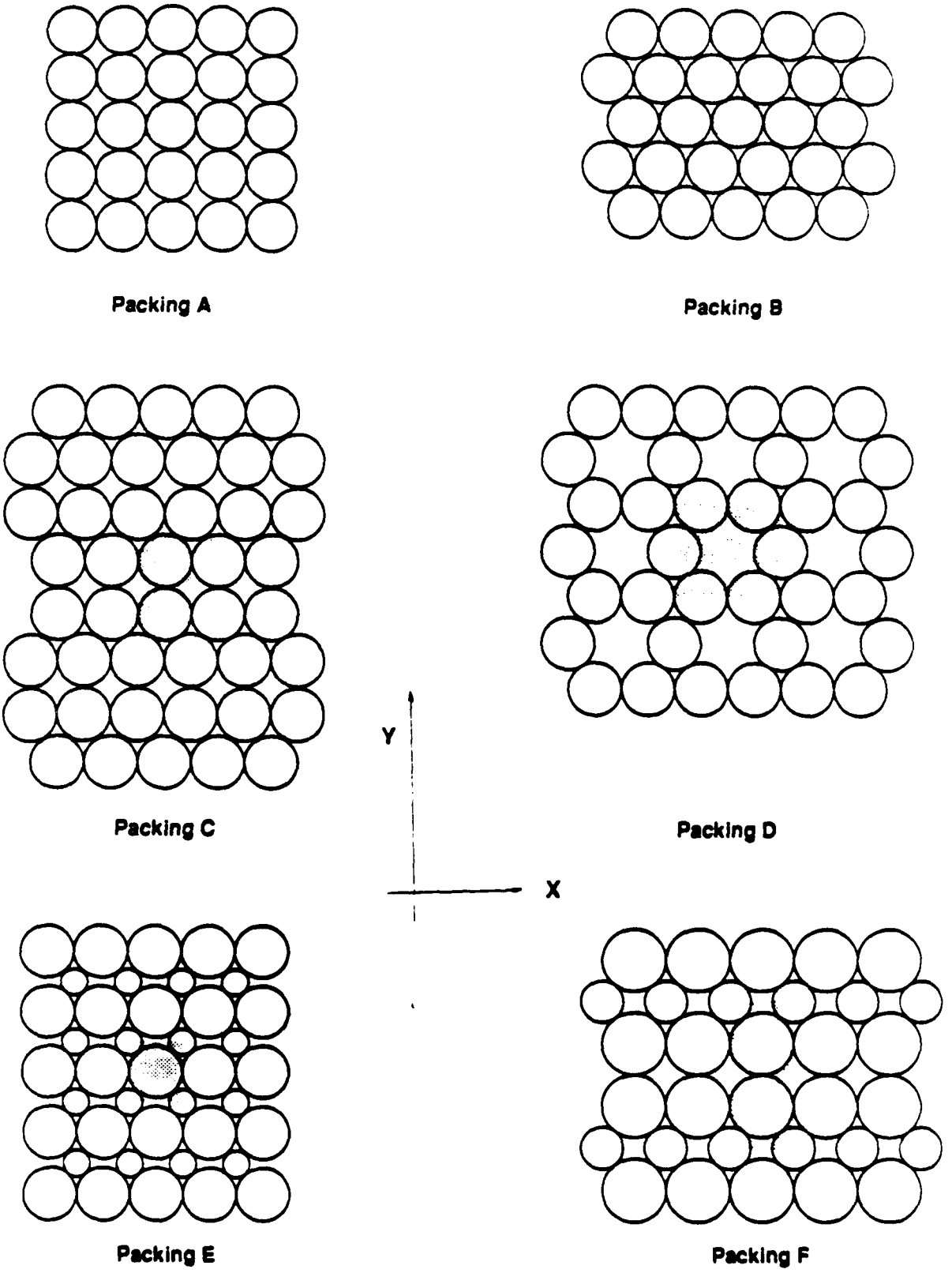

Fig. 5.2 Six regular packings of cylinders.

marked so that, from photographs, the coordinates of the center point of each circle can be digitizd to give the contact normal distribution.

5.3 STRESS PATHS

The stress path applied to the sample is a shear test with fixed principal stress axis as illustrated in Fig. 5.3 on a normalized deviatoric stress vs shear stress plot. All tests start with isotropic initial stress state, represented by the point of origin in Fig. 5.3. An initial isotropic stress of 2.5 psi is used for all the tests. Then the incremental stress of 0.5 psi is applied to the sample in a direction with an angle α inclined from Y-axis such that the principal stress axis is rotated by an angle of α, with the major principal stress σ_1= 3.0 psi and the minor principal stress σ_3=2.5 psi. For each packing, tests were conducted for the following α angles (0^o, 15^o, 22.5^o, 30.0^o, 37.5^o, and 45.0^o).

5.4 TEST DEVIATION

Each test was repeated several times to evaluate the test variability. The coefficients of variations of the measured strains ε_x, ε_y and shear strain ε_{xy} are found to be about 20%, 18% and 15% for ε_x, ε_y and ε_{xy} respectively. The scatter may be caused by many factors. In addition to the factors associated with loading system and apparatus, one factor identified is that the rods are not perfectly circular and equal in diameter. Thus identical samples are not possible to be reconstructed.

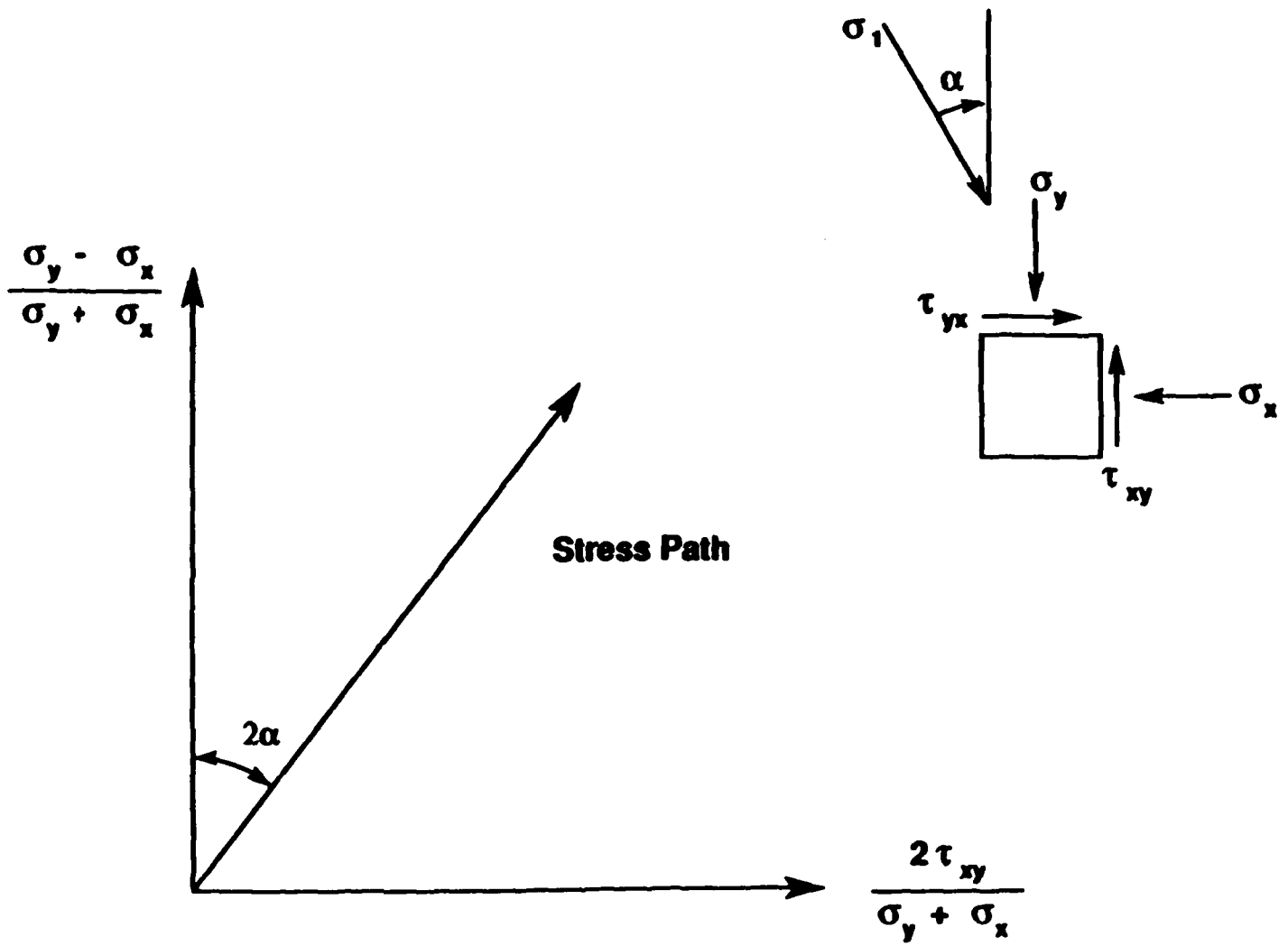

Fig. 5.3 Stress paths followed for the tests on rod assemblies.

Chapter 6

COMPARISON OF THEORETICAL AND EXPERIMENTAL RESULTS

Verification of the theory is carried out by comparing the theoretical computations with the measured experimental results. Comparisons are made with the experimental results from the tests on rod assemblies in directional shear box. Comparisons are also made with test results from glass balls assembly in a resonant column device and tests on sands under low amplitude waves. Response under different initial stress conditions are also computed and compared with measured trends.

6.1 COMPARISON WITH EXPERIMENTS ON ROD ASSEMBLIES

6.1.1 Regular packings

To compare with the experimental results, the response of the six regular packings (shown Fig. 5.2) under the loading conditions discussed above were computed using the theory. The values of the constants used for theoretical computations in this work are: G = 15000 psi (105000 kN/m^2), Ψ = 2.5, ν = 0.1, and $\phi_\mu = 15^o$.

The apparent deformation modulus of a packing is defined by

$$E = \frac{\Delta\sigma_\alpha}{\varepsilon_\alpha} \tag{6.1}$$

where $\Delta\sigma_\alpha$ is the incremental stress in the direction α, ε_α is the measured incremental normal strain in the direction α, calculated from measured deformation of test box. The apparent Poisson's ratio can be given by

$$\mu = \frac{-\varepsilon_\alpha}{\varepsilon_{\alpha+90}} \tag{6.2}$$

where $\varepsilon_{\alpha+90}$ is the normal strain measured in the direction perpendicular to that of ε_{α}. Normal strains ε_{α} and $\varepsilon_{\alpha+90}$ are not necessary the principal strains.

Figs. 6.1 and 6.2 show the apparent moduli and apparent Poisson's ratio for the six packings respectively. The measured results are compared with the predicted theoretical results for various values of α on polar coordinates.

Packing A (square packing) is most stiff when loaded in the direction of Y-axis. When it is loaded in the diagonal direction (i.e., as α becomes to 45 degree) the modulus is minimum while the Poisson's ratio is maximum. Packing B (hexagonal packing) behaves isotropically. Both moduli and Poisson's ratio are equal in all directions. Packing C, is a mixture of square packing and hexagonal packing. Remarkably the modulus and Poisson's ratio of packing C are average of those of packing A and packing B. Packing D shows the similar isotropic behavior as that of packing B, however, the magnitude of the modulus of packing D is much smaller than packing B. Both packing E and F are two-sized packings. Their moduli and Poisson's ratios are anisotropic. More detailed comparisons are included in Chang and Misra 1988a, Chang, Misra and Xue 1988.

6.1.2 **Random packings**

Two types of random packings are used for the experiments. Random packing A is made of one size rods with total number of contacts N=1372, the void ratio e=0.179, and the coordination number $\bar{m}$=5.06. Random packing B consists of rods of two different sizes with total number of contact N=1991, the void ratio e=0.179, and the coordination number $\bar{m}$=4.75. The distribution of the branch vectors. vector joining the centroids of two particles in contact, is shown in Figs. 6.3 and 6.4 for the two packings.

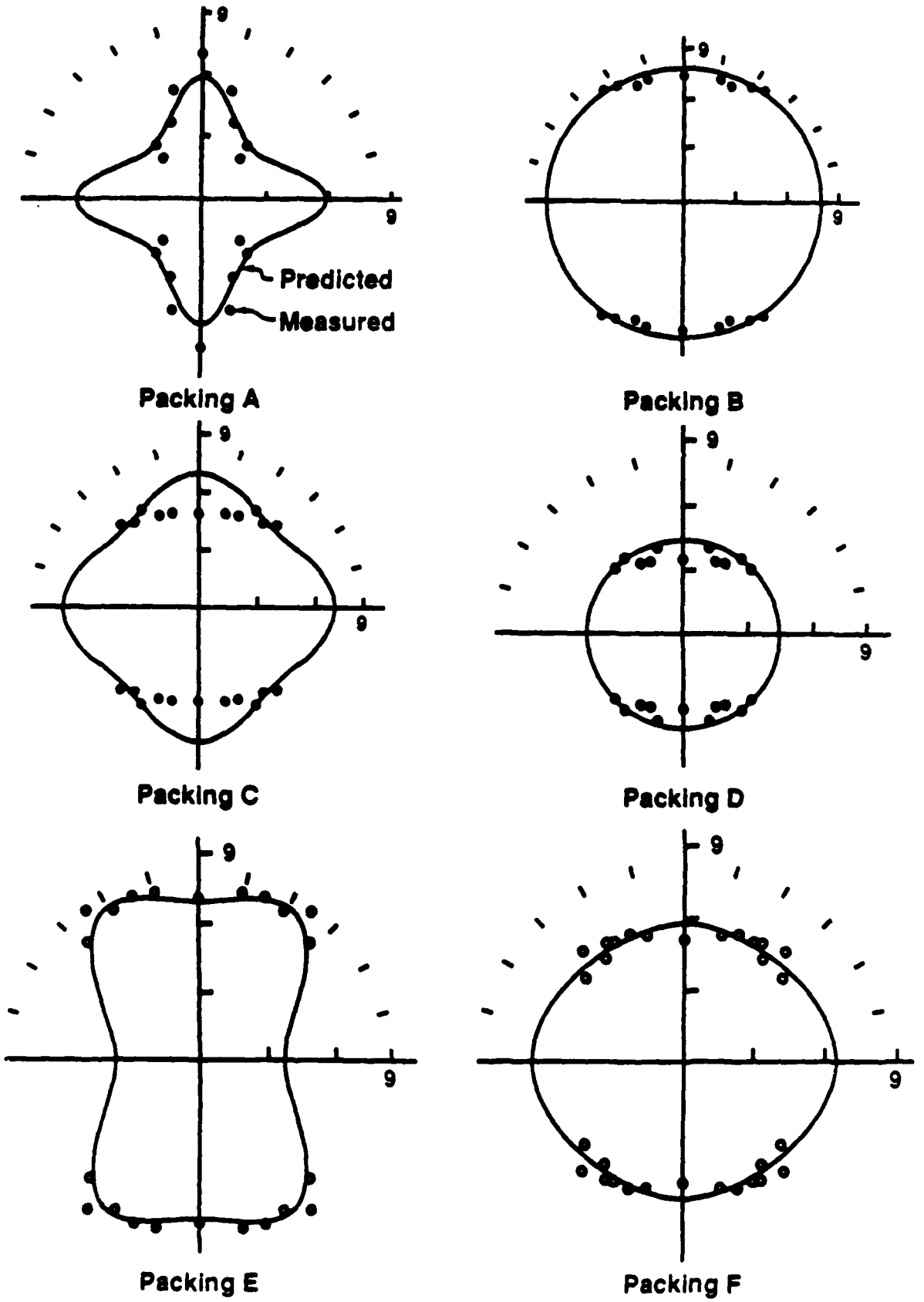

Fig. 6.1 Apparent moduli with direction for the six regular packings.

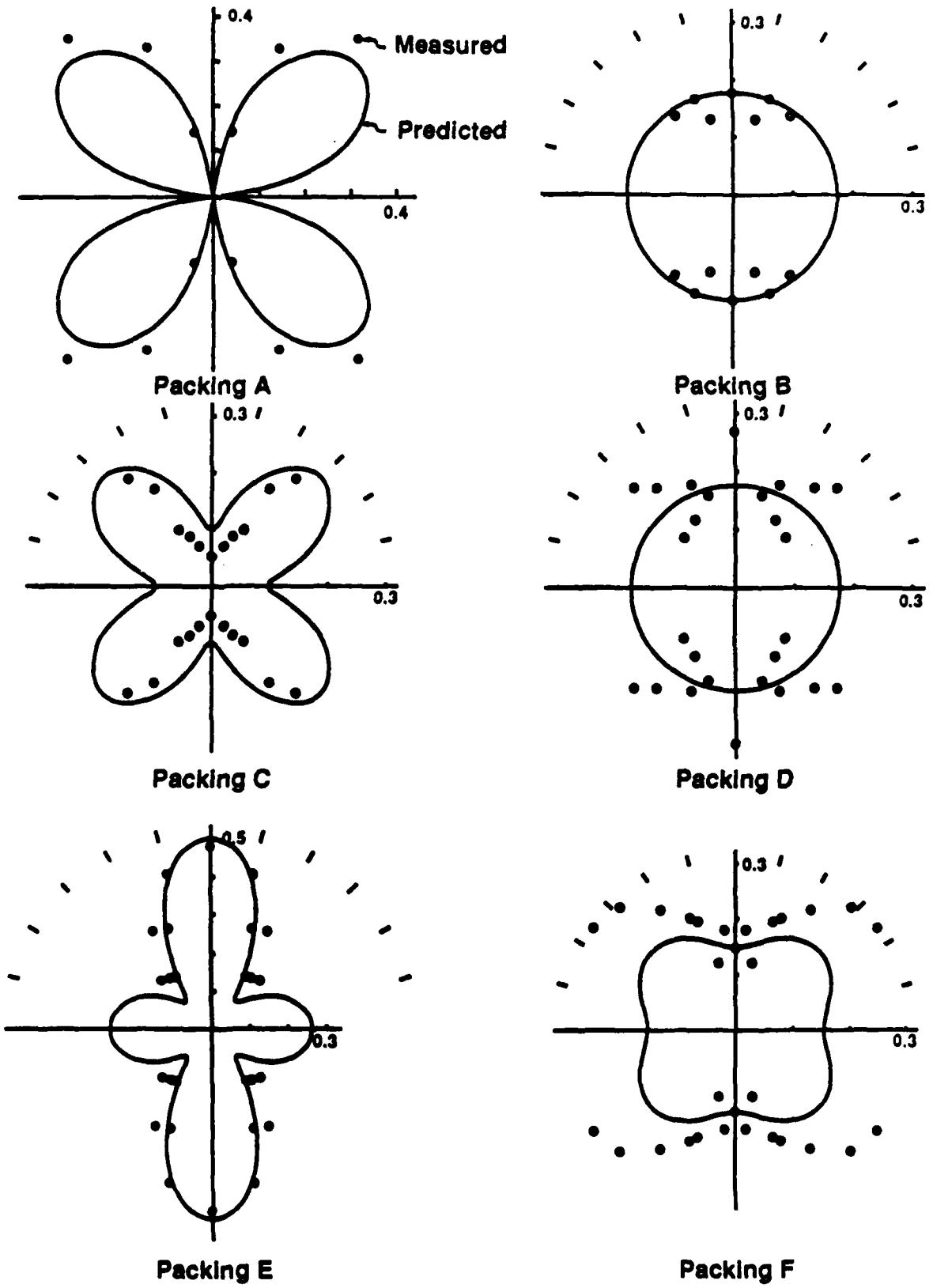

Fig. 6.2 Apparent Poisson's ratio with direction for the six regular packings.

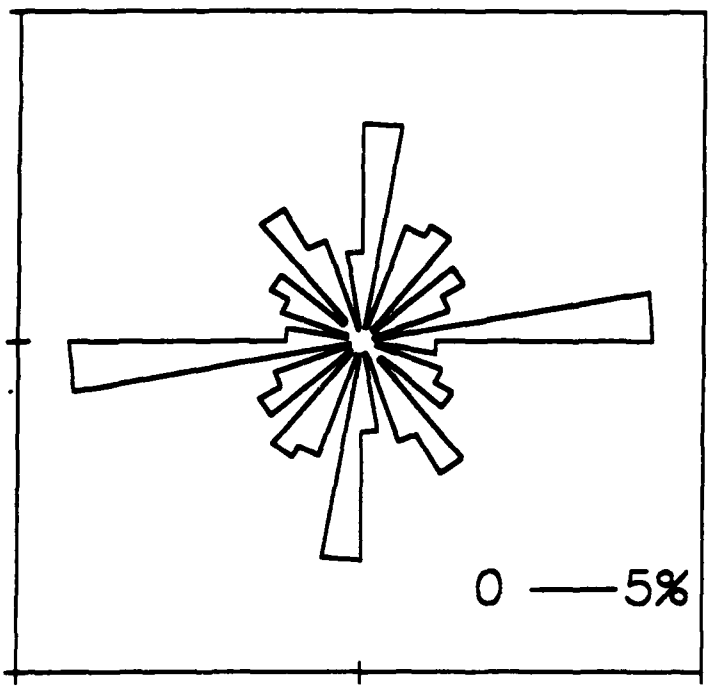

BRANCH LENGTH = 0.5 in.
NO. OF CONTACTS = 1372

Fig. 6.3 Branch vector distribution for one size random packing of cylinders.

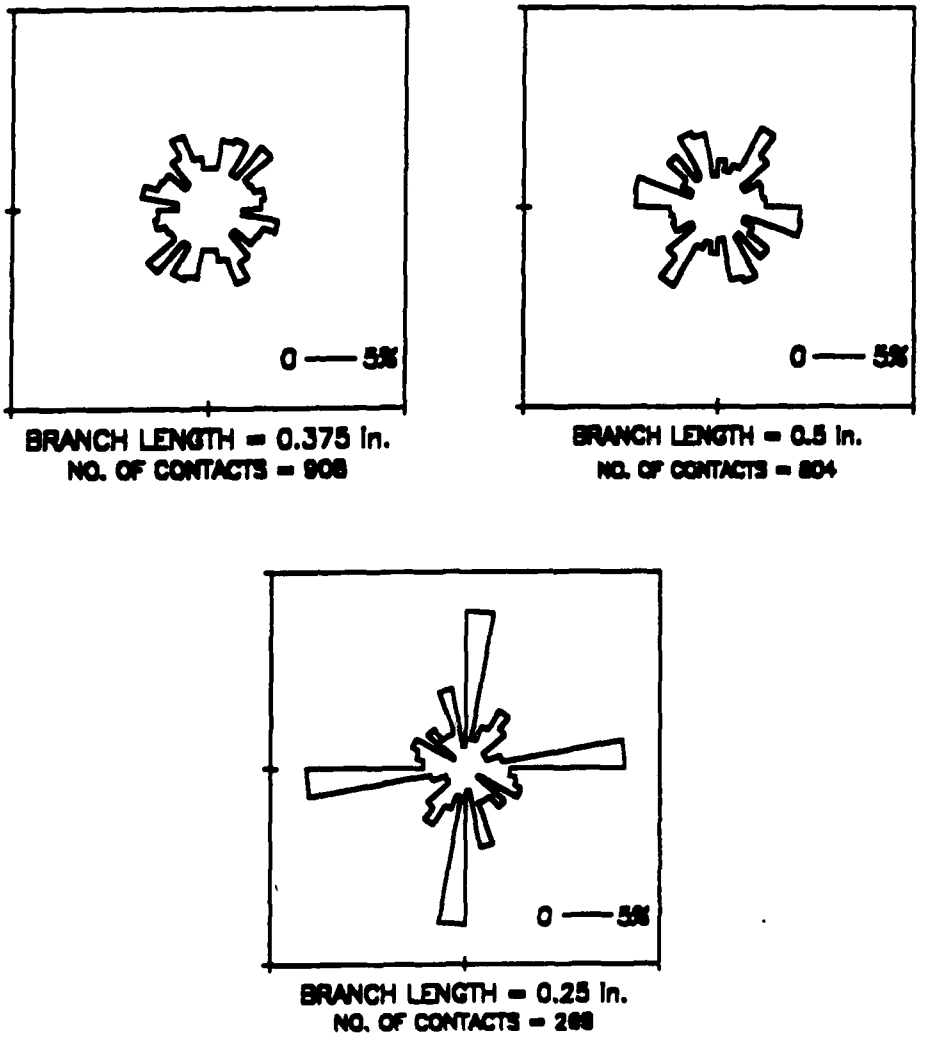

Fig. 6.4 Branch vector distribution for two-size random packing of cylinders.

Clearly the branch vector is two times the contact position vector for the case of one size packings.

To compare with the experimental results, three sets of values of the constants to represent stiff, soft and average response were used. The values of the constants used are: $\tilde{G}$ = 40000 psi (280000 kN/m^2), Ψ = 1.0 for stiff packing; $\tilde{G}$ = 15000 psi (105000 kN/m^2), Ψ = 2.5 for soft packing; and $\tilde{G}$ = 25000 psi (175000 kN/m^2), Ψ = 2.0 for the best fit of the experimental results. For all the computations the value of ν is 0.1, and ϕ_μ is 15^o.

The theoretical predictions and the measured strains are shown in Figs. 6.5 and 6.6 plotted against the direction of the principal stress axis α. The measured data is completely bounded within the predicted response. The theory gives reasonable predictions of the trend. Measured strain ε_{xx} shows more scatter since it is very small in magnitude and therefore expected to have more measurement errors.

6.2 COMPARISON WITH EXPERIMENTS ON GLASS BALLS IN RESONANT COLUMN DEVICE

To evaluate the applicability of the theory, the theoretical results are also compared with the experimentally observed shear modulus of packings of uniform glass balls from resonant column method. A confining pressure is initially applied to the cylindrical samples made of glass balls contained within a rubber membrane (Yanagisawa 1983). Then the torsional oscillation is applied on the top of the specimen to develop a shear wave transmitted through the specimen. The shear wave velocity or the shear modulus of the material can be obtained from the observed resonant frequency and the dimensions of the specimen.

Since no information is available on the packing structure, for computing the theoretical results we assume that the packing of glass balls

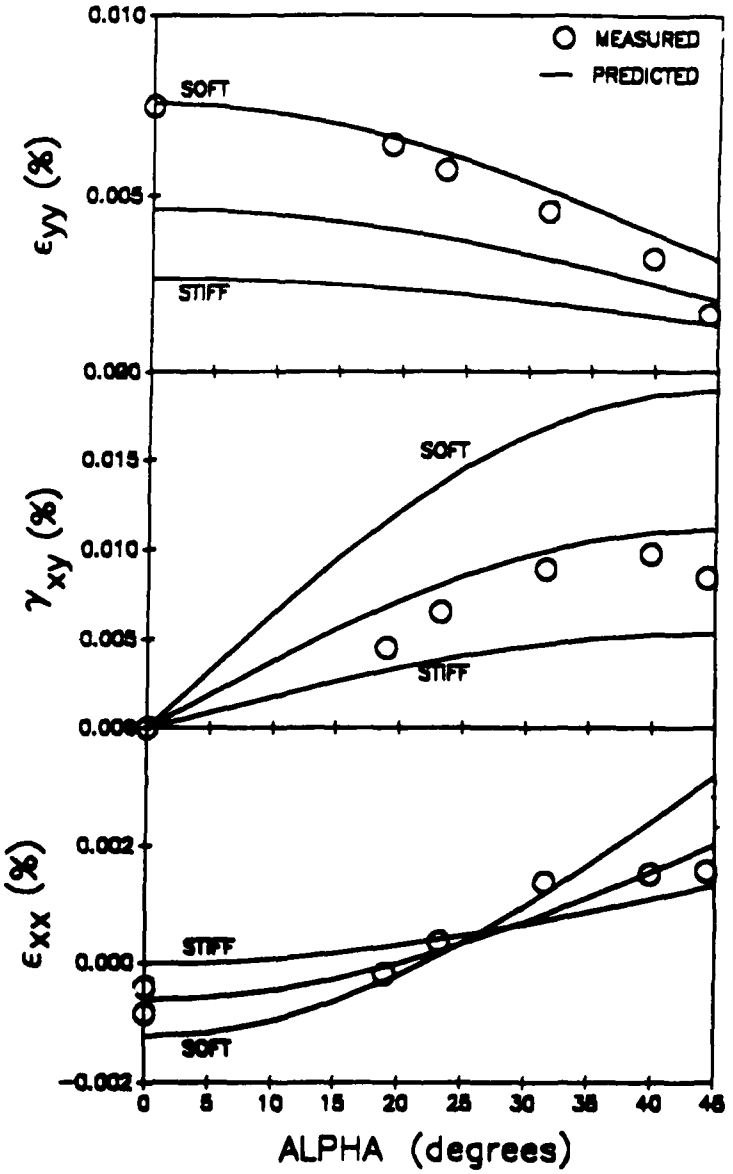

Fig. 6.5 Strains versus direction of major principal stress axis α for the one-size random packing of cylinders.

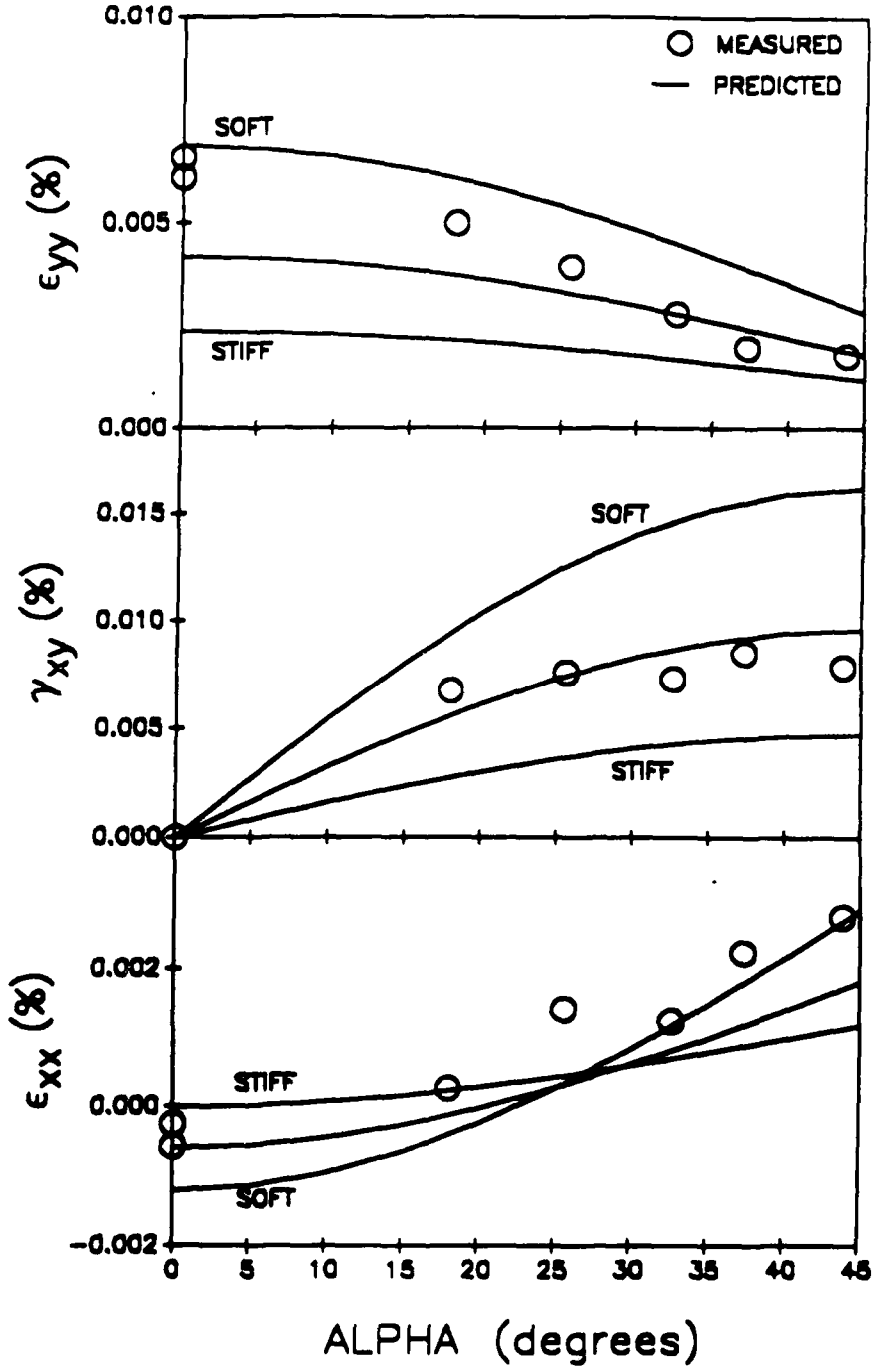

Fig. 6.6 Strains versus direction of major principal stress axis α for the two-size random packing of cylinders.

is statistically isotropic. The shear modulus is taken to be 5.75×10^6 psi (4.0×10^7 kN/m^2) and the Poisson's Ratio is 0.13 for glass. The relationship between the co-ordination number $\bar{m}$ and the void ratio e used in this prediction is given by Eq. 4.2 by Yanagisawa (1983).

Fig. 6.7 shows the comparison of the predicted and measured moduli for the packing of glass balls. As can be seen from Fig. 6.7, the shear modulus is influenced significantly by the confining pressure σ_c. The experimental values show that the shear moduli increase in proportion to the 0.42 power of the confining pressure σ_c while in theory the power is 0.33.

6.3 COMPARISON WITH EXPERIMENTS ON SANDS UNDER LOW AMPLITUDE WAVES

6.3.1 Comparison with empirical equation

Applicability of the theory is also evaluated by comparing with an empirical equation for sand which was obtained from the results of a large amount of resonant column tests conducted on dry Ottawa sands by Hardin and Black (1968). The shear modulus of sands is empirically expressed as

$$G = \frac{2630\ (2.17-e)^2\ \sigma^{1/2}}{(\ 1 + e\ )} \tag{6.3}$$

where the shear modulus G of the packing and the confining stress σ are expressed in psi.

A modified form of contact law for rough inelastic non-conforming bodies (Chang, Misra and Somasega 1988a) is used for computing the theoretical results for the comparison purposes. The shear modulus of material used is 7.5×10^6 psi (5.2×10^7 kN/m^2) and the Poisson's ratio ν is 0.13. The relationship between $\bar{m}$ and e used here is in the following form,

$$e = \frac{(23 - \bar{m})}{25} \tag{6.4}$$

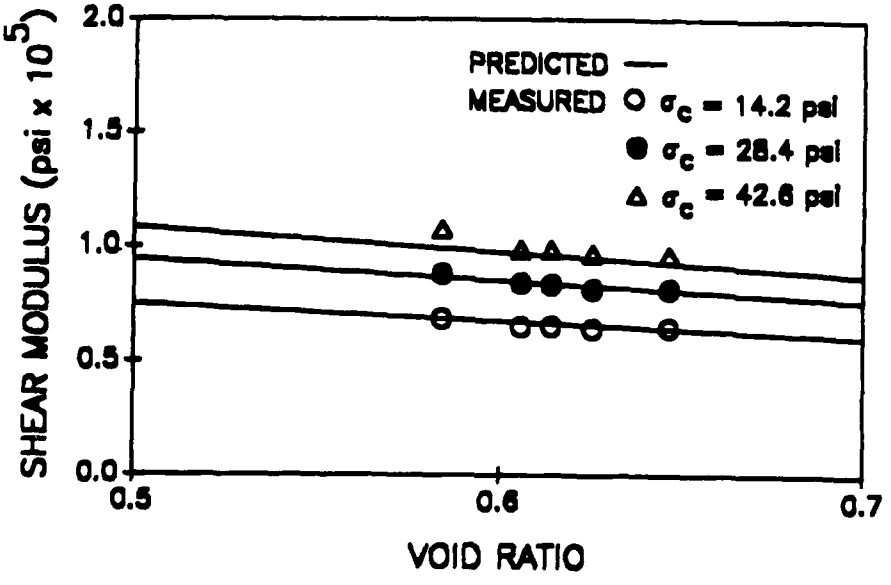

Fig. 6.7 Comparison of predicted and measured shear moduli for a packing of glass balls.

Eq. 6.4 is shown in Fig. 6.8 compared with measured data on void ratio and coordination number. For convenience, a linear line is used to fit the measured data. The comparison between the shear moduli obtained from the theory and the empirical equation is shown in Fig. 6.9.

6.3.2 Effect of initial stress conditions

The initial stress condition is an important factor influencing the mechanical behavior of a packing. A closed-form solution is difficult to obtain for initial stress conditions other than isotropic for the reason that the forces vary at contacts and hence the contact stiffness is different for each contact.

Moduli of an isotropic packing are computed for different initial stress conditions. The different initial stress conditions are represented by points of stress state lying on three stress paths shown in Fig. 6.10 namely, 1) compression path, 2) constant mean path, and 3) reduced compression path. Initially, stresses $\sigma_1 = \sigma_2 = \sigma_3 = 10$ psi (69 kN/m^2). In path 1, the axial stress σ_1 is increased while the confining stress ($\sigma_2 = \sigma_3$) is kept constant. In path 2, σ_1 is increased and σ_2 and $\sigma_3$decreased while the mean stress is kept constant. In path 3, σ_3 and σ_2 are decreased while the vertical stress σ_1 is kept constant. The moduli are computed using $G = 7.5 \times 10^6$psi (5.2×10^7 kN/m^2), $\nu = 0.13$, and $\phi_\mu = 24^\circ$. It is observed that, under these stress conditions, the packing exhibits cross-isotropic behavior with properties symmetrical about z axis.

The computed Young's moduli in the vertical direction are shown in Fig. 6.11 for the three stress paths. With an increase of stress ratio, the moduli in the vertical direction increase for the compression path while the moduli decrease for the reduced compression path. For the constant mean path, the moduli decreases only slightly. This trend is in agreement with

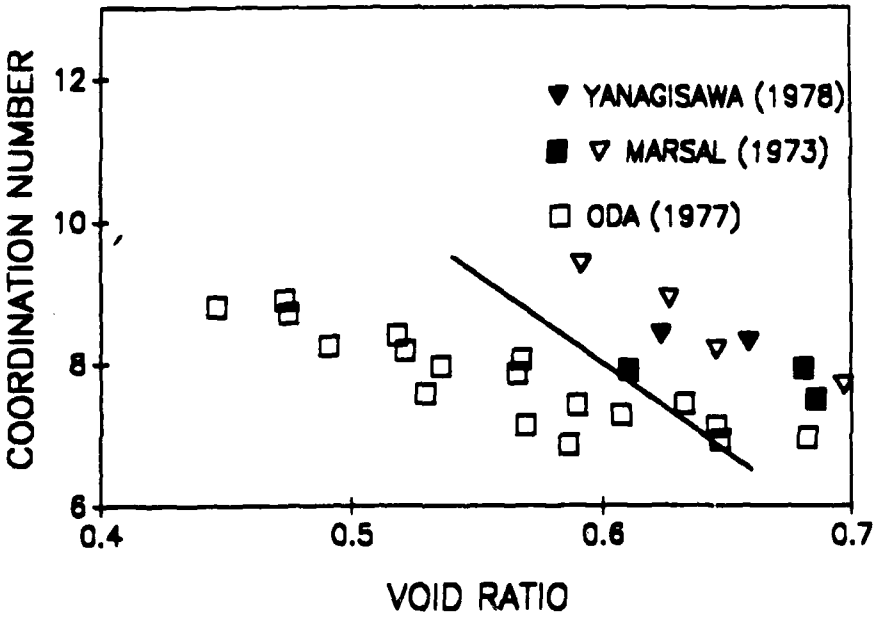

Fig. 6.8 Co-ordination number vs void ratio for Eq. 6.4 compared with the experimental data.

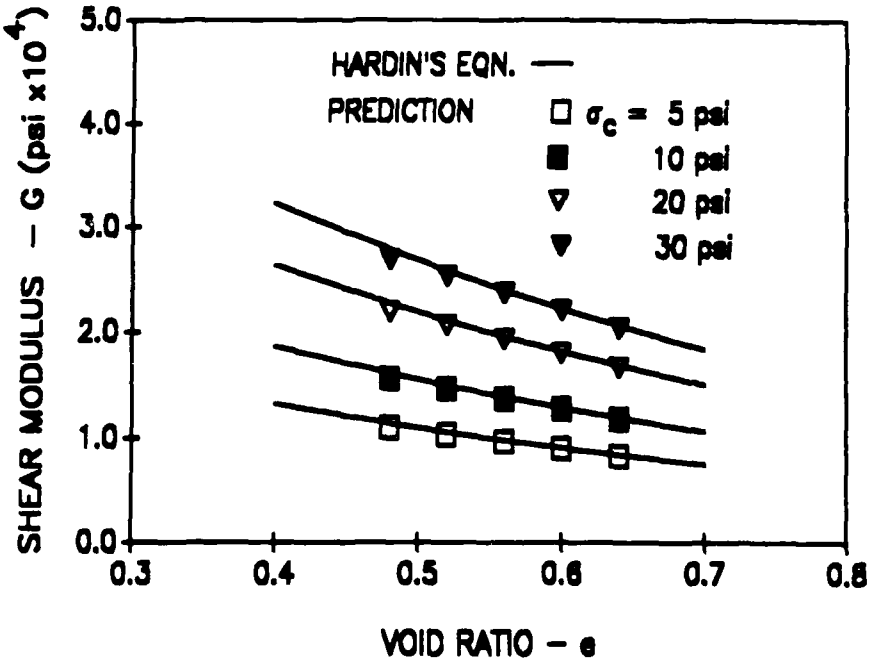

Fig. 6.9 Comparison of shear moduli obtained from the theory with that obtained from Hardin's equation.

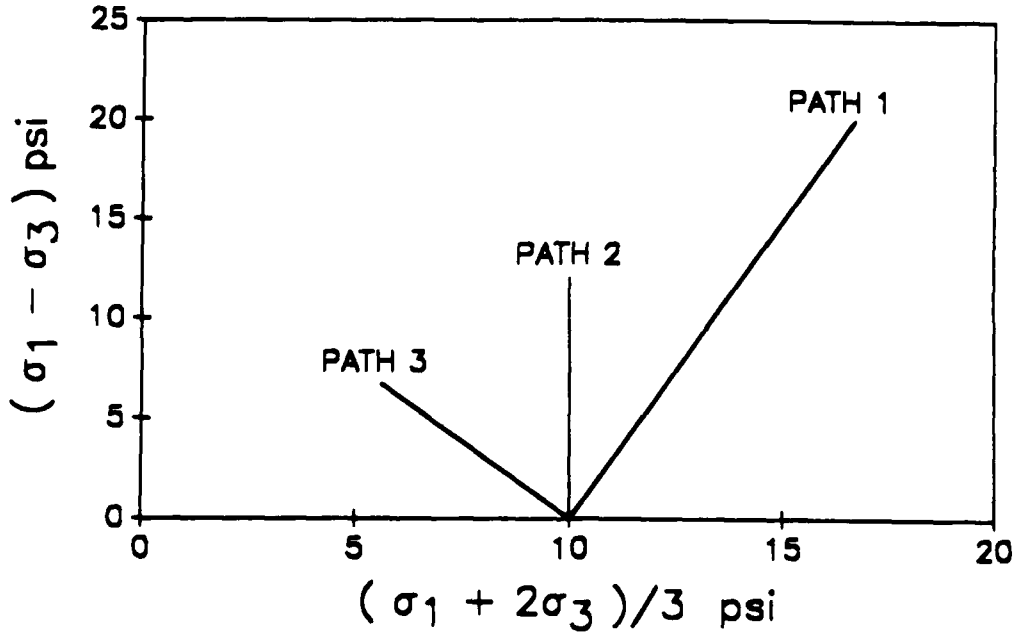

Fig. 6.10 Stress paths for different initial stress conditions.

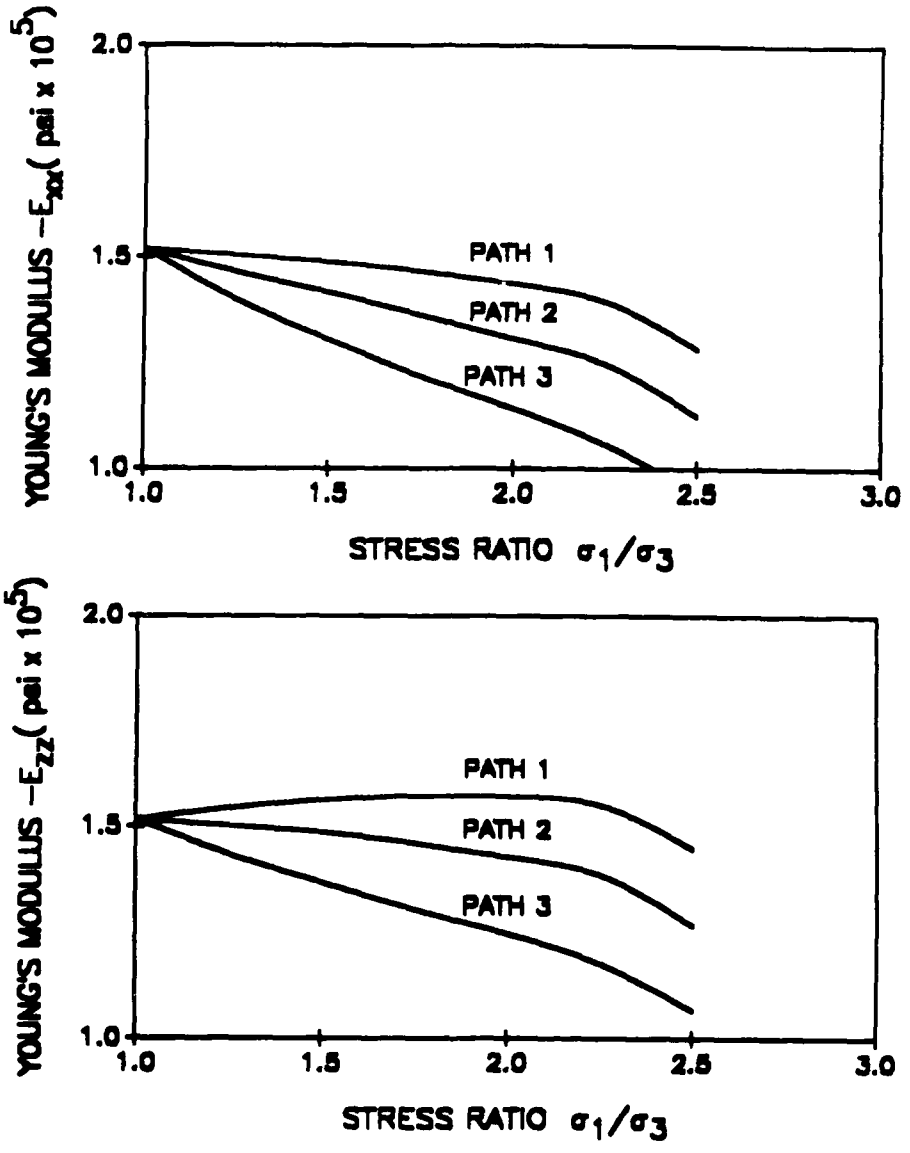

Fig. 6.11 Young's moduli, E_{zz} and E_{xx}, versus stress ratio σ_1/σ_3.

the trend observed in the experimental tests by Yanagisawa (1983). For stress ratio σ_1/σ_3 greater than 2.3, the Young's moduli and the shear moduli show appreciable decrease because the shear force exceeds the contact shear strength for many contacts. For comparison, the computed Young's moduli in the horizontal direction and the shear moduli are also shown in Fig. 6.11 and 6.12 respectively.

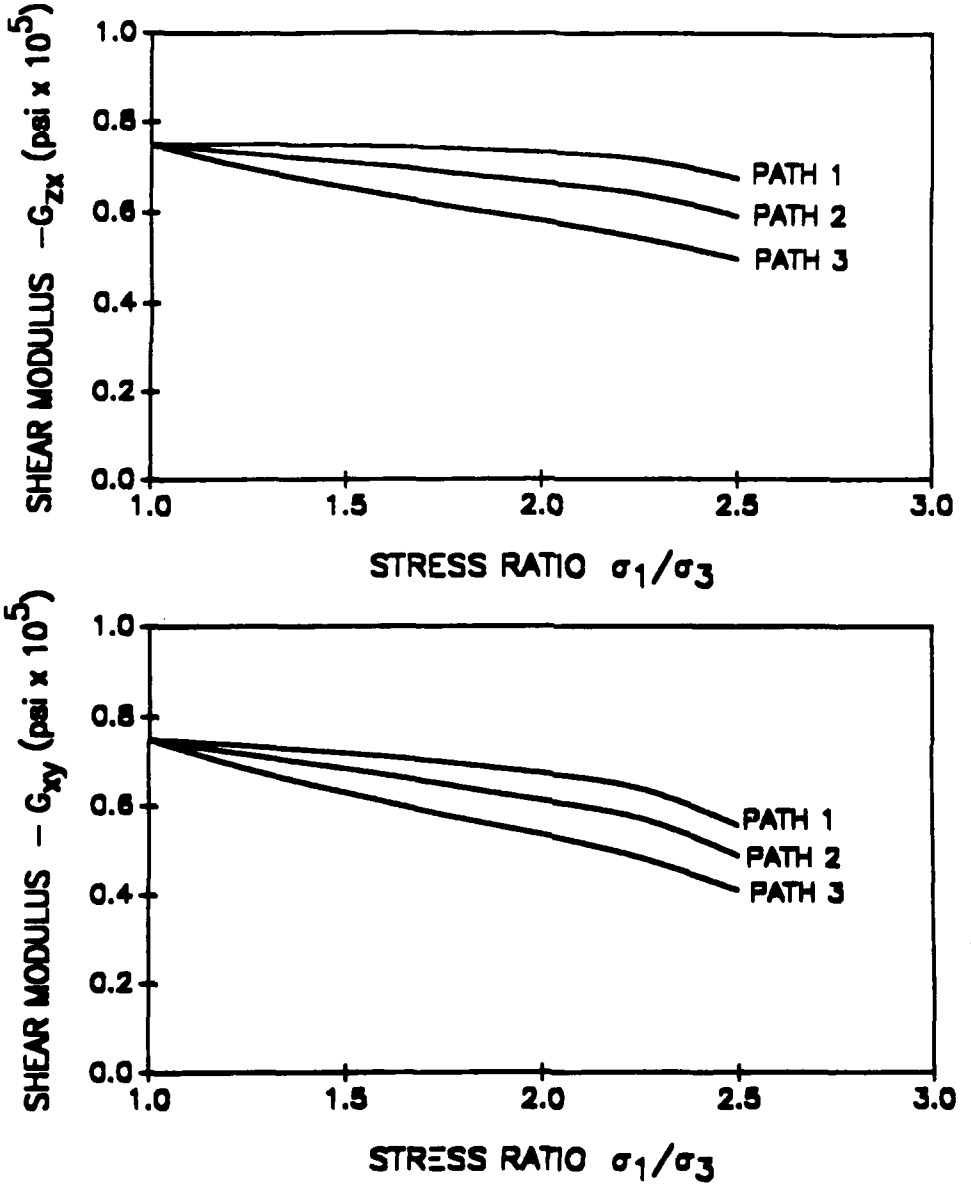

Fig. 6.12 Shear moduli, G_{zx} and G_{xy}, versus stress ratio σ_1/σ_3.

REFERENCES

Abramowitz, M. and Stegun, I.A. (1965), Handbook of Mathematical Functions, Dover, New York.

Batchelor, G.W. and O'Brien, R.W. (1977), "Thermal or Electrical Conduction Through a Granular Material," Proceedings Royal Society London, A355, pp. 313-333.

Bathurst, R.J. and Rothenburg, L. (1988), "Micromechanical Aspects of Isotropic Granular Assemblies with Linear Contact Interactions," Journal of Applied Mechanics, ASME, pp. 17-23.

Butkov, E. (1968), Mathematical Physics, John Wiley, New York.

Chang, C.S. (1988), "Micromechanical Modelling of Constitutive Equation for Granular Material," Micromechanics of Granular Materials, Elsevier Science Publishers, Edited by J.T.Jenkins and M.Satake. (in print)

Chang, C.S., and Misra, A. (1988a), "Theoretical and Experimental Study of Regular Packings of Granules," Journal of Engineering Mechanics Division, ASCE. (in print)

Chang, C.S., and Misra, A. (1988b), "Constitutive Relations for Packings of Spheres," (submitted).

Chang, C.S., and Misra, A. (1988c), "Influence of Packing Structure on the Mechanics of Granular Matter," (submitted).

Chang, C.S., and Misra, A. (1988d), "Fabric and Stiffness Properties of Anisotropic Granular Packings," (submitted).

Chang, C.S., Misra, A. and Xue, J.H. (1988), "Model Tesellations Applied to Study the Mechanics of Packings Made of Multi-Sized Particles," (submitted).

Chang, C.S., Somasegarasundaram, S. and Misra, A. (1988), "Implications of Micro-structure on Elastic Moduli of Particulated Mass," (submitted).

Christoffersen, J., Mehrabadi, M.M. and Nemat-Nasser, S. (1981), "A Micromechanical Description of Granualar Material Behavior," Journal of Applied Mechanics, ASME, pp. 339-344.

Cowin, S.C. (1985), "The Relationship Between the Elasticity Tensor and the Fabric Tensor," Mechanics of Materials. Vol. 4, pp. 137-147.

Field, W.G. (1963), "Towards the statistical definition of a granular mass," Proc. 4th Aust. and N.Z. Conf. on Soil Mech., pp. 143-148.

Filep, L. (1936), Egyenlo gombokbol allo halmazok, Vizugyi Kozlemenyek.

Finney, J.L. (1970), "Random Packings and Structure of Simple Liquids I. The Geometry of Random Close Packing," Proc. Roy. Soc. A, Vol. 319, pp. 479-493.

Gray, W.A. (1968), The Packing of Solid Particles, Chapman and Hall, London.

Hardin, B.O., and Richart, F.E. (1963), "Elastic wave velocities in granular soils," Journ. Soil Mech. & Found. Div., Proc. ASCE, Vol.89 No.SM1, pp. 33-41.

Johnson, K.L. (1985), Contact Mechanics, Cambridge University Press, London.

Kanatani, K. (1984), "Distribution of Directional Data and Fabric Tensors," International Journal of Engineering Sciences, Vol. 22, pp. 149-164.

Kishino, Y. (1978), "Statistical Consideration on Deformation Characteristics of Granular Materials," Proceedings, US-Japan Seminar on Continuum Mechanical and Statistical Approaches in the Mechanics of Granular Materials, Ed. S.C. Cowin and M. Satake, pp. 114-122.

Marsal, R.J. (1973), "Mechanical properties of rockfill," Embankment Dam Engineering, pp. 109-145.

Mindlin, R.D. (1949), "Compliances of Two Elastic Bodies in Contact," Journal of Applied Mechanics, ASME, pp. 259-268.

Mindlin, R.D. and Deresiewicz, H. (1953), "Elastic Spheres in Contact Under Varying Oblique Forces," Journal of Applied Mechanics, ASME, pp. 327-344.

Nye, J.F. (1957), Physical Properties of Crystals, Oxford, London.

Oda, M. (1977), "Co-ordination number and its relation to shear strength of granular material," Soils and Found., Vol. 17, No.2, pp. 29-42.

Oda, M., Nemat-Nasser, S. and Meharabadi, M.M. (1982), "A Statistical Study of Fabric in a Random Assembly of Spherical Granules," International Journal for Numerical and Analytical Methods in Geomechanics, Vol. 6, pp. 77-94.

Rothenburg, L. and Selvadurai, A.P.S. (1981), "Micromechanical Definition of the Cauchy Stress Tensor for Particulate Media," Mechanics of Structured Media, Ed. A.P.S. Selvadurai, Elsevier, pp. 469-486.

Satake, M. (1982), "Fabric Tensor in Granular Materials," Proceedings, IUTAM Symposium on Deformation and Failure of Granular Materials, Eds. P.A. Vermeer and H.J. Luger, A.A. Balkema, Delft, pp. 63-68.

Shahinpoor, M. (1983), Advances in the Mechanics and the Flow of Granular Materials, Gulf Publishing Company, Houston, Texas.

Smith, W.O., Foote, P.D. and Busang, P.F. (1929), "Packing of homogeneous spheres," Phys. Rev., Vol.34, pp. 1271-1274.

Thornton, C. and Randall, C.W. (1988), "Developments in Computer Simulation of Dissipative Solid Particle Systems," Micromechanics of Granular Materials, Elsevier Science Publishers, Edited by J.T.Jenkins and M.Satake. (in print)

Truesdell, C. and Toupin, R.A. (1960), The Classical Field Theories, Handbuch der Physik, Ed. S. Flugge, Vol. III/1, Springer Verlag, Berlin.

Truesdell, C. and Noll, W. (1965), The Non-linear Field Theories of Mechanics, Handbuch der Physik, Ed. S. Flugge, Vol. III/3, Springer Verlag, Berlin.

Xue, J.H. (1988), "Experimental Study on Mechanical Behavior of Idealized Granular Media," Master's Project Report Submitted to the University of Massachusetts in partial fulfillment of the requirements of the degree of Master of Science.

Yanagisawa, E. (1983), "Influence of void ratio and stress condition on the dynamic shear modulus of granular media," Adv. in the Mechanics and the Flow of Granular Materials, Ed. M. Shahinpoor, pp. 947-960.